J. Fluid Mech. (2024), *vol*. 999, A55, doi:10.1017/jfm.2024.927

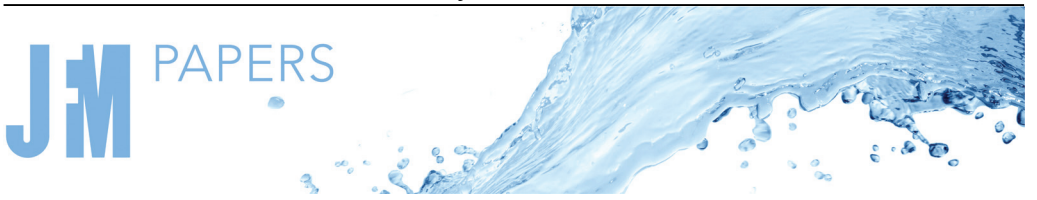

On dewetting and concentration evolution of thin binary fluid films

J.A. Diez[1], **A.G. González**[1],† **and L. Kondic**[2]

[1]Instituto de Física Arroyo Seco, Universidad Nacional del Centro de la Provincia de Buenos Aires, and CIFICEN-CONICET-CICPBA, Pinto 399, 7000, Tandil, Argentina

[2]Department of Mathematical Sciences and Center for Applied Mathematics and Statistics, New Jersey Institute of Technology, Newark, NJ 07102, USA

(Received 5 January 2024; revised 21 September 2024; accepted 22 September 2024)

We study the stability and dewetting dynamics of a thin free-surface film composed of two miscible liquids placed on a solid substrate. Our study focuses on the development of a self-consistent model such that the mixture concentration influences both free-surface and wetting energies. By assuming a simple relation between these energies and the bulk and surface concentrations, we analyse their effect on the concentration distribution and dewetting down to the equilibrium film thickness determined by the fluid–solid interaction potential. The model, developed within the gradient dynamics formulation, includes the dependence of the free-surface energy on surface concentration leading to the Marangoni effect, while a composition-dependent Hamaker constant describes the wetting energy resulting from the fluid–solid interaction. We analyse the restrictions that must be fulfilled to ensure an equilibrium state for a flat film of a binary fluid. Then, we proceed by studying its linear stability. First, we consider the Marangoni effect while assuming that wetting energy depends only on the fluid thickness. Then, we include a dependence of wetting energy on concentration and study its effects. We find that the linear stability results compare very well with those of numerical simulations of the full nonlinear problem applied to the particular case of a binary melted metal alloy, even close to breakup times. Therefore, in practice, most of the evolution can be studied by using the linear theory, simplifying the problem considerably.

Key words: thin films, multiphase flow, coupled diffusion and flow

1. Introduction

Binary fluids are relevant in numerous settings and have been explored extensively. The modelling of fluid flows combined with concentration evolution requires solving

† Email address for correspondence: aggonzal@exa.unicen.edu.ar

of the Navier–Stokes equations coupled with convective and diffusive effects that may be composition-dependent. Extensive research has been carried out for systems of this type, particularly in the context of oil-recovery and core–annular flows (Joseph & Renardy 1992*a*,*b*; Joseph *et al.* 1997).

In recent decades, there has been significant interest in the flow dynamics and stability on much smaller scales, from micro down to nanometric. In particular, various types of flows and related instabilities have been considered in the context of free-surface thin films deposited on solid substrates. Short length scales and flow geometries involve additional complications associated with the presence of free surfaces. There are, however, also simplifications which could be considered. For many thin-film systems, an asymptotic long-wave expansion is appropriate, and significant advances have been reached by using this approach, see Oron, Davis & Bankoff (1997) and Craster & Matar (2009) for reviews. In the present context, it is relevant to note the relation between the resulting thin film equation and the Cahn–Hilliard formulation (Cahn & Hilliard 1958; Cahn 1965) as pointed out by Mitlin (1993). In the context of binary films of thicknesses larger than nanometres, substantial progress has been achieved in various contexts; the reader is referred to the introduction of Shklyaev, Nepomnyashchy & Oron (2009) for an instructive overview of the relevant works; here, we just list a few examples. Two-layer films of immiscible films have been considered extensively (Pototsky *et al.* 2004, 2005), as well as those covered by surfactants (Thiele, Archer & Plapp 2012; Morozov, Oron & Nepomnyashchy 2015). In an extensive body of work, various authors (Podolny, Oron & Nepomnyashchy 2005; Shklyaev, Nepomnyashchy & Oron 2013, 2014) studied miscible binary fluids exposed to heating; in some of these works, both solutal and thermal Marangoni effects were considered, leading to complicated evolution and instability development. Wetting effects in binary fluids were considered in the recent work by Areshi *et al.* (2024).

On even shorter (nanometric) length scales, fluid–solid interaction forces that, in general, are concentration-dependent become relevant. Most of the work in this direction has been carried out using the gradient dynamics formulation (Thiele, Velarde & Neuffer 2001; Thiele 2011; Thiele, Todorova & Lopez 2013; Huth *et al.* 2015; Sarika *et al.* 2015; Sarika, Tomar & Basu 2016; Thiele, Archer & Pismen 2016) that we will consider in the present work as well. We should also mention the early work by Clarke (2005), which is not fully consistent with the gradient dynamics approach. Other works considering similar approaches include the ones by Köpf, Gurevich & Friedrich (2009), Köpf *et al.* (2010) and Náraigh & Thiffeault (2010), as well as the work by Xu, Thiele & Qian (2015), which provides further development in terms of symmetric solvent–solute approach. In mathematical terms, the gradient dynamics formulation leads to coupled partial differential equations describing the evolving film thickness and the concentration of two phases (in the case of binary systems). The reader is referred in particular to a mini-review (Thiele 2018) for a concise overview of the relevance of the formulation of the problem at hand within the gradient dynamics framework, as well as for a discussion of various problems that were (and were not) considered in the context of gradient dynamics.

There are numerous important binary or ternary systems with concentration evolution, with only some recent examples mentioned here (Karpitschka, Liebig & Riegler 2017; Mao *et al.* 2019; Chao *et al.* 2022), where the formulation that we consider in the present paper is applicable widely. However, for definiteness and also to be able to connect the results to existing physical experiments, we consider liquid metal films of nanoscale thickness as a model system. Such films are of particular interest for the applications requiring nano-patterning, such as solar cells, plasmonics-related set-ups, sensing and detection, among others (see Hughes, Menumerov & Neretina (2017), Makarov *et al.* (2016)

for reviews). One approach to pattern formation is self- and directed instability involving melting the films by application of laser pulses of duration measured on a nanosecond time scale (or even shorter); while melted, films evolve as Newtonian fluids and form drops which solidify into particles once the temperature drops below the melting point. We focus on the evolution while the metal is in a liquid state and refer the interested reader to a different problem of solid-state dynamics; see recent works focusing on that regime (Khenner 2018; Khenner & Henner 2020), as well as a review article (Thompson 2012).

Liquid state dewetting of metal films with other geometries is present in many situations, and significant progress has been reached in understanding elemental (single fluid) systems; see Kondic *et al.* (2020) for a recent review. Bimetallic films were also considered both experimentally and theoretically in earlier work (Diez *et al.* 2021) which already produced interesting new results and insights, particularly regarding the competition of film thickness instability and the concentration distribution. In the present work, we remove some significant simplifications of this earlier work and focus on understanding the influence of the (solutal) Marangoni effect and the concentration dependence of the fluid–solid interaction forces on the stability of the film thickness and of the concentration field.

The rest of this paper is organized as follows. In § 2 we revisit the gradient dynamics formulation by including the various contributions to the free energy of a system formed by a thin film of binary fluid and a supporting solid substrate. Then, we analyse the component terms of the resulting pressure and chemical potentials, as well as the system of evolution equations. In § 3, we find the conditions on the chemical potentials that must be fulfilled to have the base state in equilibrium. Then, in § 4, we proceed by carrying out a linear stability analysis (LSA) of such a base state. Section 5 describes the properties of the instability when the solutal Marangoni effects are considered, with the wetting energy depending only on the fluid thickness. Then, in § 6, we add a dependence of the latter on both surface and bulk concentrations. For all cases, we compare the LSA results with the full nonlinear numerical solution. Finally, in § 7, we summarize the results and discuss their implications and possible future directions.

2. Gradient dynamics formulation

We study the stability properties of a nanometric thin film composed of two miscible fluids (binary fluid) on top of a solid planar surface. Figure 1 illustrates the considered geometry. In the bulk of the film of thickness $h(x, t)$, one of the fluids (say, fluid A) has a volume fraction, $c_A(\boldsymbol{x}, z, t)$, where $\boldsymbol{x} = (x, y)$, so that its z-averaged concentration, ϕ, is

$$\phi(\boldsymbol{x}, t) = \frac{1}{h(\boldsymbol{x}, t)} \int_0^{h(\boldsymbol{x},t)} c_A(\boldsymbol{x}, z, t)\, \mathrm{d}z = \frac{\psi(\boldsymbol{x}, t)}{h(\boldsymbol{x}, t)}. \tag{2.1}$$

Then, the corresponding z-averaged concentration of fluid B is $1 - \phi$. Here, we will also use the variable

$$\psi(\boldsymbol{x}, t) = \phi(\boldsymbol{x}, t) h(\boldsymbol{x}, t), \tag{2.2}$$

which stands for the amount of fluid A inside a column of height $h(\boldsymbol{x}, t)$ and unit in-plane area.

Initially, the thickness of the mixture is h_0, and the bulk concentration of fluid A is ϕ_0, so that $\psi_0 = \phi_0 h_0$. At the free surface of the film, the fluid A is assumed to have a surface concentration, $\Gamma(\boldsymbol{x}, t)$. Analogously, the surface concentration of fluid B is $1 - \Gamma$. If $\Gamma \ll 1$, then one could think of fluid A as a soluble surfactant with surface concentration Γ and volume concentration ϕ. Conversely, if $1 - \Gamma \ll 1$, then fluid B can be thought of

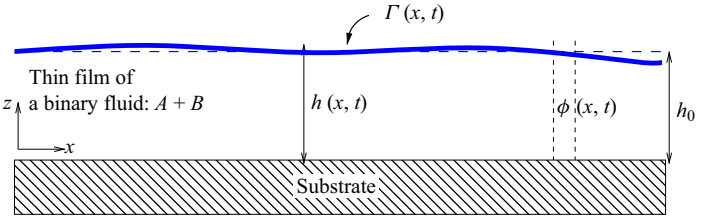

Figure 1. Sketch of the thin film–substrate system showing the main variables of the problem: thickness h, volume concentration ϕ and surface concentration Γ. Initially, the binary fluid has a volume concentration ϕ_0 of fluid A and $(1-\phi_0)$ of fluid B and a film thickness h_0.

as a surfactant. The model includes the possibility of an exchange of fluids between the surface and the bulk, but we do not consider a mass exchange with the gaseous phase above the film. Note that conservation of mass at the free surface implies $\Gamma\,\mathrm{d}S_f = \tilde{\Gamma}\,\mathrm{d}S$, where dS_f is the element of the free surface, $h(\boldsymbol{x}, t)$, and $\tilde{\Gamma}$ is the projected concentration on the plane element $\mathrm{d}\mathcal{A} = \mathrm{d}x\,\mathrm{d}y$. Thus, we have $\tilde{\Gamma} = \Gamma\xi$, with $\xi = \sqrt{1+|\nabla h|^2}$.

We proceed by presenting a brief overview of the formulation developed in Thiele *et al.* (2016), where the gradient dynamics approach is extended to describe the non-equilibrium dissipative dynamics of thin-film systems and to cast the dynamic equations into a form that reproduces Onsager's reciprocity relations (Thiele *et al.* 2016). We start by considering the corresponding free energy functional

$$\mathcal{F} = \int \left[f(h, \Gamma, \phi) + hg(\phi) + \xi g_s(\Gamma) + \frac{\sigma}{2} h|\nabla(\phi)|^2 + \frac{\sigma_s}{2}|\nabla(\Gamma)|^2 \right] \mathrm{d}\mathcal{A}, \tag{2.3}$$

where f is the wetting energy, g the bulk mixing energy and g_s the surface energy.

The first term in (2.3) corresponds to the energy per unit surface of the interatomic/molecular interaction between the liquid in the film and the solid substrate (e.g. van der Waals interaction). We write it in general form as

$$f(h, \Gamma, \phi) = K\gamma_{ref} F(h, \Gamma, \phi), \quad K = \frac{\mathcal{H}_{ref}}{6\pi\gamma_{ref} h_e^2}, \tag{2.4}$$

where h_e is the equilibrium film thickness, and γ_{ref}, $\mathcal{H}_{ref}$ are the reference values of surface tension and the Hamaker constant, respectively. Since both concentrations ϕ and Γ, as well as ψ, refer to fluid A, we choose $\gamma_{ref} = \gamma_B$ and $\mathcal{H}_{ref} = \mathcal{H}_B$. In general, we consider a dependence on both Γ and ϕ since atoms/molecules in the bulk as well as at the free surface take part in the interaction with atoms/molecules in the substrate. This contribution is relevant when the film thickness is nanometric. The function $g(\phi)$ in the second term of (2.3) represents the bulk Gibbs energy per unit volume. For convenience, we write it as

$$g(\phi) = \mathcal{E} G(\phi), \quad \mathcal{E} = \frac{k_B T}{a^3}, \tag{2.5}$$

where G is a non-dimensional function and a is an atomic/molecular length scale in the fluid bulk (e.g. the radius of a spherical atom/molecule Thiele 2011).

The third term in (2.3) stands for the free energy contribution due to the presence of molecules of both fluids at the free surface. We write it as

$$g_s(\Gamma) = \mathcal{E}_s G_s(\Gamma), \quad \mathcal{E}_s = \frac{k_B T}{a_s^2}, \tag{2.6}$$

where a_s is a molecular size associated with the interphase molecular structure. According to the formulation in Thiele *et al.* (2016) (e.g. in their (B27)), the energy functions g_s and

Variable	Symbol	In units of
in-plane coordinates	x, y	ℓ
thickness, aver. bulk concentration	h, ψ	$\bar{h}_0$
time	t	$3\eta_0\ell^4/(\gamma_{ref}\bar{h}_0^3)$
surface tension	$\hat{\gamma}$	γ_{ref}
surface and bulk concentrations	Γ, ϕ	1
free energy	$\mathcal{F}$	$\gamma_{ref}\ell^2$
pressure	p	$\gamma_{ref}\bar{h}_0/\ell^2$
bulk chemical potential	μ	$\gamma_{ref}/\bar{h}_0$
surface chemical potential	μ_s	γ_{ref}

Table 1. Scales of the non-dimensional variables used in the dimensionless equations.

f define the general expression of surface tension as

$$\gamma(h, \Gamma, \phi) = g_s - \Gamma\frac{\partial g_s}{\partial \Gamma} - \Gamma\frac{\partial f}{\partial \Gamma} - \frac{\sigma_s}{2}|\boldsymbol{\nabla}\Gamma|^2 + \sigma_s\Gamma\nabla^2\Gamma. \tag{2.7}$$

The dependence of γ on the surface concentration, Γ, is not surprising. For instance, the first two terms correspond to the usual Marangoni effect. However, the fluid–solid interaction energy (i.e. wetting energy) given by third term on the right-hand side of (2.7)) introduces a dependence on both ϕ and h, leading to additional effects, since the fluid–solid interaction forces may also influence the free-surface tension.

The last two terms in (2.3) stand for the energetic contribution of gradients in both bulk, ϕ, and surface, Γ, concentrations, where σ (energy per unit length) and σ_s (energy) denote the interfacial stiffness of the diffuse interface between the pure fluids in the bulk and at the free surface, respectively (Thiele, Madruga & Frastia 2007).

From now on, we consider a non-dimensional formulation by expressing the thicknesses h and ψ in units of a characteristic thickness of the film, $\bar{h}_0$. The in-plane coordinates (x, y) are expressed in units of an arbitrary length ℓ, and time t is in units of

$$t_c = \frac{3\eta\ell^4}{\gamma_{ref}\bar{h}_0{}^3}, \tag{2.8}$$

where η is the viscosity of the film. Therefore, the non-dimensional free energy in (2.3), in units of $\gamma_{ref}\ell^2$, takes the form

$$\mathcal{F} = \int \mathcal{F}_s\,\mathrm{d}S = \int \left[KF(h, \Gamma, \phi) + \beta h G(\phi) + \xi\beta_s G_s(\Gamma) + \frac{\Sigma}{2}h|\boldsymbol{\nabla}\phi|^2 + \frac{\Sigma_s}{2}|\boldsymbol{\nabla}\Gamma|^2\right]\mathrm{d}\mathcal{A}, \tag{2.9}$$

where the parameters are defined as

$$\Sigma = \frac{\sigma\bar{h}_0}{\gamma_{ref}\ell^2}, \quad \Sigma_s = \frac{\sigma_s}{\gamma_{ref}\ell^2}, \quad \beta = \frac{k_B T\bar{h}_0}{\gamma_{ref}a^3}, \quad \beta_s = \frac{k_B T}{\gamma_{ref}a_s^2}. \tag{2.10a–d}$$

Table 1 gives a summary of the dimensional parameters and their combinations that have been used for the non-dimensionalization.

In the following, we consider the general formulation of the gradient dynamics for a given expression of the total free energy, $\mathcal{F}$. Thus, we write the coupled evolution

equations ((42) to (45) developed in Thiele *et al.* 2016) for the three fields in the framework of linear non-equilibrium thermodynamics and the long-wave approximation ($\xi \approx 1$, requiring that we choose $h_0 \ll \ell$) as

$$\frac{\partial h}{\partial t} + \boldsymbol{\nabla}\cdot\left[-h^3\boldsymbol{\nabla}\frac{\delta\mathcal{F}}{\delta h} - \frac{3}{2}h^2\Gamma\boldsymbol{\nabla}\frac{\delta\mathcal{F}}{\delta\Gamma} - h^2\psi\boldsymbol{\nabla}\frac{\delta\mathcal{F}}{\delta\psi}\right] = 0, \tag{2.11a}$$

$$\frac{\partial\Gamma}{\partial t} + \boldsymbol{\nabla}\cdot\left[-\frac{3}{2}h^2\Gamma\boldsymbol{\nabla}\frac{\delta\mathcal{F}}{\delta h} - (3h\Gamma^2 + 3D_s\Gamma)\boldsymbol{\nabla}\frac{\delta\mathcal{F}}{\delta\Gamma} - \frac{3}{2}h\psi\Gamma\boldsymbol{\nabla}\frac{\delta\mathcal{F}}{\delta\psi}\right] = -\tilde{J}_{ad}, \tag{2.11b}$$

$$\frac{\partial\psi}{\partial t} + \boldsymbol{\nabla}\cdot\left[-h^2\psi\boldsymbol{\nabla}\frac{\delta\mathcal{F}}{\delta h} - \frac{3}{2}h\psi\Gamma\boldsymbol{\nabla}\frac{\delta\mathcal{F}}{\delta\Gamma} - (h\psi^2 + 3D\psi)\boldsymbol{\nabla}\frac{\delta\mathcal{F}}{\delta\psi}\right] = J_{ad}. \tag{2.11c}$$

Here, we have defined the non-dimensional diffusivities

$$D = \frac{M}{\bar{h}_0^2} = \frac{\mathcal{D}\eta}{\mathcal{E}\bar{h}_0^2} = \frac{\mathcal{D}\eta a^3}{k_BT\bar{h}_0^2}, \tag{2.12}$$

$$D_s = \frac{M_s}{\bar{h}_0} = \frac{\mathcal{D}_s\eta}{\mathcal{E}_s\bar{h}_0} = \frac{\mathcal{D}_s\eta a_s^2}{k_BT\bar{h}_0} = \frac{\mathcal{D}_s}{\mathcal{D}}\frac{a_s^3}{a^3}\frac{D}{s}, \tag{2.13}$$

$$s = \frac{a_s}{\bar{h}_0}, \tag{2.14}$$

where M and M_s are the molecular mobilities in the bulk and the surface, respectively, which are related to the molecular energy densities $\mathcal{E}$ and $\mathcal{E}_s$ through the molecular diffusion coefficients of the binary fluid for the bulk and surface, $\mathcal{D}$ and $\mathcal{D}_s$, respectively. Note that the definition of $\mathcal{D}$ agrees with the Stokes–Einstein relation if $M = a^2/6\pi$. We note that the value of $\mathcal{D}$ is not sufficient to determine M, since one still needs to estimate a. This quantity is of the nanometric order, and it is related to diffusion processes in the bulk. One also needs the value of a_s, which is associated with adsorption and desorption processes in the surface, so that it is expected to be even smaller than a (Diamant & Andelman 1996). It is usual to consider $a \approx a_s$, and we use this approximation here; also, we assume that $\mathcal{D}_s \approx \mathcal{D}$. Therefore, under these assumptions, we write

$$D_s = \frac{D}{s}, \quad \beta_s = s\beta, \quad \Sigma_s = s\Sigma. \tag{2.15a–c}$$

Here, we follow the approach discussed in Diez *et al.* (2021) and weight average the parameters of interest. For example, the viscosity, η, and the diffusivity, $\mathcal{D}$, of the mixture are given by a weighted average of those of the components, i.e.

$$\eta = \eta_A\phi_0 + (1-\phi_0)\eta_B, \quad \mathcal{D} = \mathcal{D}_A\phi_0 + (1-\phi_0)\mathcal{D}_B, \tag{2.16a,b}$$

where $\eta_{A,B}$ and $\mathcal{D}_{A,B}$ are the corresponding values for the pure fluids.

The right-hand sides of (2.11*b*) and (2.11*c*) correspond to the adsorption–desorption flux between the bulk and the surface, given by (see e.g. (38) and (55) in Thiele *et al.* 2016)

$$\tilde{J}_{ad} = 3D_s\Gamma\left(\frac{1}{s}\frac{\delta\mathcal{F}}{\delta\Gamma} - \frac{\delta\mathcal{F}}{\delta\psi}\right) = 3D_s\Gamma\left(\frac{\mu_s}{s} - \mu\right) = \frac{J_{ad}}{s}. \tag{2.17}$$

Based on the energy functional specified by (2.9), and under the long-wave approximation, we have (see the Appendix in Thiele *et al.* 2016)

$$p \equiv \frac{\delta \mathcal{F}}{\delta h} = -\nabla[\hat{\gamma}(\Gamma, h)\nabla h] + K\frac{\partial F}{\partial h} - K\frac{\psi}{h^2}\frac{\partial F}{\partial \phi} + \beta\left(G - \frac{\psi}{h}\frac{\partial G}{\partial \phi}\right) + \Sigma\left(-\frac{2\psi}{h^3}\nabla h\cdot\nabla\psi + \frac{|\nabla\psi|^2}{2h^2} + \frac{3\psi^2}{2h^4}|\nabla h|^2 - \frac{\psi^2}{h^3}\nabla^2 h + \frac{\psi}{h^2}\nabla^2\psi\right), \tag{2.18}$$

$$\mu_s \equiv \frac{\delta \mathcal{F}}{\delta \Gamma} = \beta_s\frac{\partial G_s}{\partial \Gamma} + K\frac{\partial F}{\partial \Gamma} - \Sigma_s\nabla^2\Gamma, \tag{2.19}$$

$$\mu \equiv \frac{\delta \mathcal{F}}{\delta \psi} = \beta\frac{\partial G}{\partial \phi} + \frac{K}{h}\frac{\partial F}{\partial \phi} + \Sigma\left(-\frac{\psi}{h^3}|\nabla h|^2 + \frac{\nabla h\cdot\nabla\psi}{h^2} + \frac{\psi}{h^2}\nabla^2 h - \frac{\nabla^2\psi}{h}\right), \tag{2.20}$$

where

$$\hat{\gamma}(\Gamma, h) = \frac{\gamma}{\gamma_{ref}} = \beta_s\left(G_s - \Gamma\frac{\partial G_s}{\partial \Gamma}\right) - K\,\Gamma\frac{\partial F}{\partial \Gamma} - \frac{\Sigma_s}{2}|\nabla\Gamma|^2 + \Sigma_s\Gamma\nabla^2\Gamma, \tag{2.21}$$

is the non-dimensional version of (2.7). In (2.18)–(2.20), p stands for pressure, and μ_s, μ stand for surface and bulk chemical potentials. Here, p and μ are given in units of $\gamma_{ref}h_0/\ell^2$, and μ_s in units of γ_{ref}.

Let us now consider the physical interpretation of the terms in (2.18)–(2.20). The total pressure, p, can be written as

$$p = p_{cap} + p_{wet} + p_{osm} + p_{Kort}, \tag{2.22}$$

where the subscripts stand for capillary, wetting, osmotic and Korteweg pressures, and

$$\left.\begin{aligned} p_{cap} &= -\nabla[\hat{\gamma}(\Gamma, h)\nabla h], \quad p_{wet} = K\left(\frac{\partial F}{\partial h} - \frac{\psi}{h^2}\frac{\partial F}{\partial \phi}\right), \quad p_{osm} = \beta\left(G - \frac{\psi}{h}\frac{\partial G}{\partial \phi}\right), \\ p_{Kort} &= \Sigma\left(-\frac{2\psi}{h^3}\nabla h\cdot\nabla\psi + \frac{1}{2h^2}|\nabla\psi|^2 + \frac{3\psi^2}{2h^4}|\nabla h|^2 - \frac{\psi^2}{h^3}\nabla^2 h + \frac{\psi}{h^2}\nabla^2\psi\right). \end{aligned}\right\} \tag{2.23}$$

The last pressure component, related to diffuse interfaces, can also be found in the literature (see e.g. Doi 2011; Thiele *et al.* 2013) in terms of ϕ as

$$p_{Kort} = \Sigma\left(\frac{1}{2}|\nabla\phi|^2 + \frac{\phi}{h}\nabla h\cdot\nabla\phi + \phi\nabla^2\phi\right). \tag{2.24}$$

The surface chemical potential, μ_s, see (2.19), includes the contributions due to the Marangoni effects, i.e. the dependence of surface tension, γ, on surface concentration, Γ (see (2.21)). These contributions can be separated as

$$\mu_s = \mu_{s,osm} + \mu_{s,wet} + \mu_{s,diff}, \tag{2.25}$$

where

$$\mu_{s,osm} = \beta_s\frac{\partial G_s}{\partial \Gamma}, \quad \mu_{s,wet} = K\frac{\partial F}{\partial \Gamma}, \quad \mu_{s,diff} = -\Sigma_s\nabla^2\Gamma, \tag{2.26a–c}$$

and the subscripts stand for osmotic, wetting and diffusive interface potentials. Thus, the first one accounts for the variation of the surface energy with respect to the surface

concentration, the second one for the variation of the wetting energy with the surface concentration and the third one for the contribution of a diffuse interface at the surface.

Finally, the bulk chemical potential, μ, in (2.20) has three contributions

$$\mu = \mu_{wet} + \mu_{osm} + \mu_{diff}, \tag{2.27}$$

where

$$\mu_{wet} = \frac{K}{h}\frac{\partial F}{\partial \phi}, \quad \mu_{osm} = \beta \frac{\partial G}{\partial \phi}, \tag{2.28a,b}$$

$$\mu_{diff} = -\frac{\Sigma}{h}\left(\frac{\psi}{h^2}|\nabla h|^2 - \frac{1}{h}\nabla h \cdot \nabla \psi - \frac{\psi}{h}\nabla^2 h + \nabla^2 \psi\right) = -\frac{\Sigma}{h}\nabla \cdot (h \nabla \phi). \tag{2.29}$$

This completes the formulation of the problem. In order to simplify the presentation, in what follows we write (2.11*a*)–(2.11*c*) in matrix form as

$$\partial_t \boldsymbol{\Lambda} - \nabla \cdot (\boldsymbol{Q} \nabla \boldsymbol{P}) = \boldsymbol{J}, \tag{2.30}$$

where

$$\boldsymbol{\Lambda} = \begin{pmatrix} h \\ \Gamma \\ \psi \end{pmatrix}, \quad \boldsymbol{P} = \frac{\delta \mathcal{F}}{\delta \boldsymbol{\Lambda}} = \begin{pmatrix} \delta \mathcal{F}/\delta h \\ \delta \mathcal{F}/\delta \Gamma \\ \delta \mathcal{F}/\delta \psi \end{pmatrix} = \begin{pmatrix} p \\ \mu_s \\ \mu \end{pmatrix}, \tag{2.31a,b}$$

and the matrix of mobility coefficients is

$$\boldsymbol{Q} = \begin{pmatrix} h^3 & \frac{3}{2}h^2\Gamma & h^2\psi \\ \frac{3}{2}h^2\Gamma & \left(3h^2\Gamma + 3D_s\Gamma\right) & \frac{3}{2}h\psi\Gamma \\ h^2\psi & \frac{3}{2}h\psi\Gamma & \left(h^2\psi + 3D\psi\right) \end{pmatrix}. \tag{2.32}$$

The bulk-to-surface and surface-to-bulk transfer rates on the right-hand side of (2.30) are

$$\boldsymbol{J} = -\boldsymbol{M}\frac{\delta \mathcal{F}}{\delta \boldsymbol{\Lambda}} = -\boldsymbol{M}\boldsymbol{P} = \begin{pmatrix} 0 \\ -\tilde{J}_{ad} \\ J_{ad} \end{pmatrix}, \tag{2.33}$$

where

$$\boldsymbol{M} = 3D_s\Gamma \begin{pmatrix} 0 & 0 & 0 \\ 0 & 1/s & -1 \\ 0 & -1 & s \end{pmatrix}. \tag{2.34}$$

Note that both matrices $\boldsymbol{Q}$ and $\boldsymbol{M}$ are symmetric and positive definite.

Equation (2.11*a*) is in conservative form, in agreement with the fact that the film thickness $h(\boldsymbol{x}, t)$ is a conserved field, i.e.

$$\int h(\boldsymbol{x}, t)\, \mathrm{d}\mathcal{A} = V = V_A + V_B = \text{const.}, \tag{2.35}$$

where V is the volume of the binary fluid and V_A, V_B are the volumes of the pure fluids, respectively. On the other hand, note that both (2.11*b*) and (2.11*c*) have non-zero right-hand sides, which account for the mass transfer between the surface and the bulk.

Therefore, neither $\int \Gamma(\boldsymbol{x}, t)\,\mathrm{d}S$ nor $\int \psi(\boldsymbol{x}, t)\,\mathrm{d}S$ is conserved. However, if we multiply (2.11*b*) by s and add it to (2.11*c*), we obtain

$$\frac{\partial \Psi}{\partial t} + \boldsymbol{\nabla}\cdot\left[-h^2\left(\Psi + s\frac{\Gamma}{2}\right)\boldsymbol{\nabla} p - 3\Gamma\left(\frac{h\Psi}{2} + s\frac{h\Gamma}{2} + s\,D_s\right)\boldsymbol{\nabla}\mu_s - (\Psi - s\Gamma)\left(h\Psi + s\frac{h\Gamma}{2} + 3D\right)\boldsymbol{\nabla}\mu\right] = 0, \tag{2.36}$$

which is in conservative form for

$$\Psi = \psi + s\Gamma. \tag{2.37}$$

Then,

$$\int \Psi\,\mathrm{d}\mathcal{A} = \int (\psi + s\Gamma)\,\mathrm{d}\mathcal{A} = \int \phi\,\mathrm{d}V + \int s\Gamma\,\mathrm{d}\mathcal{A} = V_A^{bulk} + V_A^{surf} = V_A = \text{const.}, \tag{2.38}$$

which also implies the conservation of V_B.

The problem formulation presented so far can be mostly found in Thiele *et al.* (2016). We now proceed with the LSA, focusing in particular on the influence of the binary nature of the considered fluid.

3. Equilibrium base state

We now consider a base state of the film as given by $\boldsymbol{\Lambda}_0 = (h_0, \Gamma_0, \psi_0)$. Then, we have

$$\partial_t \boldsymbol{\Lambda}_0 - [\boldsymbol{\nabla}\cdot(\boldsymbol{Q}_0\boldsymbol{\nabla}\boldsymbol{P}_0)] = \boldsymbol{J}_0, \tag{3.1}$$

where $\boldsymbol{Q}_0 = \boldsymbol{Q}|_{\boldsymbol{\Lambda}_0}$ and

$$\boldsymbol{J}_0 = -\boldsymbol{M}_0\boldsymbol{P}_0, \quad \boldsymbol{M}_0 = 3D_s\Gamma_0\begin{pmatrix}0 & 0 & 0\\ 0 & 1/s & -1\\ 0 & -1 & s\end{pmatrix}, \quad \boldsymbol{P}_0 = \left.\frac{\delta\mathcal{F}}{\delta\boldsymbol{\Lambda}}\right|_{\boldsymbol{\Lambda}_0} = \begin{pmatrix}p_0\\ \mu_{s,0}\\ \mu_0\end{pmatrix}. \tag{3.2}$$

For the spatially homogeneous base state considered in this work, i.e. $(p_0, \mu_{s_0}, \mu_0) = const.$, we choose $\bar{h}_0$ as the initial thickness of a flat film so that $h_0 = 1$ and Γ_0, $\psi_0 = \phi_0$ are also constants. Then, the square bracket in (3.1) trivially vanishes. Therefore, the time variation of $\boldsymbol{\Lambda}_0$ is controlled by the flux $\boldsymbol{J}_0$. To ensure a stationary base state, we must have

$$\boldsymbol{J}_0 = 3D_s\Gamma_0\left(\frac{\mu_{s,0}}{s} - \mu_0\right)\begin{pmatrix}0\\ 1\\ -s\end{pmatrix} = 0. \tag{3.3}$$

Assuming $\Gamma_0 > 0$, this equation implies

$$\mu_{s,0} = s\mu_0. \tag{3.4}$$

Thus, the surface and volumetric chemical potentials must be balanced to ensure no net transfer between surface and bulk, in agreement with steady values of ϕ_0 and Γ_0 and the assumption of the stationary base state. This condition leads to a constraint on the properties that the energy functions (G, G_s and F) must obey in the base state. In fact,

when evaluating the expressions for μ and μ_s in (2.19) and (2.20) at $\boldsymbol{\Lambda}_0 = (1, \Gamma_0, \psi_0)$, we obtain

$$\beta_s \frac{\partial G_s}{\partial \Gamma}\bigg|_{\Gamma_0} + K \frac{\partial F}{\partial \Gamma}\bigg|_{\Gamma_0} = s\beta \left.\frac{\partial G}{\partial \phi}\right|_{\phi_0} + s\, K \left.\frac{\partial F}{\partial \phi}\right|_{\phi_0}. \tag{3.5}$$

One of the simplest ways to fulfil this condition is to assume the following relations compatible with these requirements:

$$\frac{\partial G_s}{\partial \Gamma}\bigg|_{\Gamma_0} = \left.\frac{\partial G}{\partial \phi}\right|_{\phi_0}, \tag{3.6}$$

$$\frac{\partial F}{\partial \Gamma}\bigg|_{\Gamma_0} = s \left.\frac{\partial F}{\partial \phi}\right|_{\phi_0}. \tag{3.7}$$

Since we are interested in analysing a wide range of concentrations, we assume an entropic form for the volumetric free energy, namely (see e.g. Archer *et al.* 2007, 2008; Thiele *et al.* 2016)

$$G(\phi) = \phi \ln \phi + (1-\phi)\ln(1-\phi). \tag{3.8}$$

Consistently with the approach used for volumetric concentrations, we resort to a similar form for the surface free energy, namely

$$G_s(\Gamma) = \frac{1}{\beta_s} + \Gamma \ln \Gamma + (1-\Gamma)\ln(1-\Gamma). \tag{3.9}$$

Then, the surface tension of the base state, $\hat{\gamma}_0$, is given by

$$\hat{\gamma}_0 = \beta_s \left(G_s - \Gamma \frac{\partial G_s}{\partial \Gamma}\right)\bigg|_{\Gamma_0} = 1 + \beta_s \ln(1-\Gamma_0). \tag{3.10}$$

Note that, for small Γ_0, this expression reduces to the usual linear Marangoni effect, i.e. $\hat{\gamma}_0 \approx 1 - \beta_s \Gamma_0$. Since $\hat{\gamma}_0 > 0$, it must be that

$$\Gamma < \Gamma_{0,max} = 1 - \mathrm{e}^{-1/\beta_s}. \tag{3.11}$$

Moreover, Γ_0 also needs to satisfy the condition specified by (3.6) which, for G and G_s given by (3.8) and (3.9), yields

$$\Gamma_0 = \phi_0, \tag{3.12}$$

which is a simple equilibrium condition (adsorption isotherm). Different choices of G and G_s lead to more complex isotherms, such as the Langmuir and Frumkin relations (see e.g. Thiele *et al.* 2016).

Let us now consider the wetting energy, F, that depends on both Γ and ϕ. We propose a factorized expression for F in the form

$$F(h, \Gamma, \phi) = \frac{\mathcal{H}(\Phi)}{\mathcal{H}_{ref}} \hat{F}(h), \tag{3.13}$$

where we define

$$\Phi = \phi + \frac{s}{h}\Gamma. \tag{3.14}$$

Note that this combination is of the same type as that used to define Ψ in (2.37), since $\Phi = \Psi/h$. We point out that the condition expressed by (3.7) is automatically satisfied

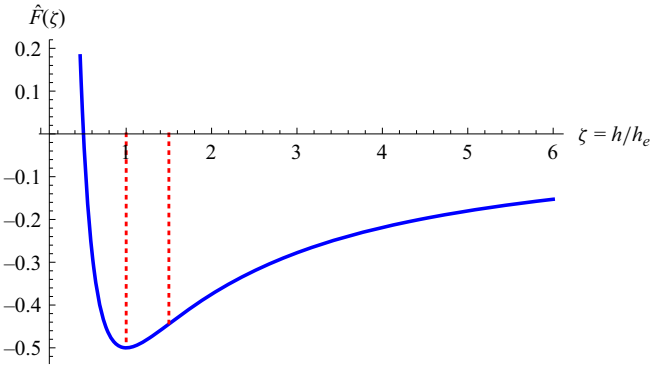

Figure 2. Fluid–solid interaction energy, $\hat{F}(\zeta)$, as a function of $\zeta = h/h_e$ for $n = 3$ and $m = 2$. The vertical dotted red lines indicate the points where $\hat{F}' = 0$ ($\zeta = 1$) and $\hat{F}'' = 0$ ($\zeta = \mathrm{e}^{\ln(m/n)/(m-n)} = 1.5$).

by this factorized form. Here, $\mathcal{H}(\Phi)$ is a Hamaker constant (for simplicity we assume the same constant for both attractive and repulsive forces). Also, we assume that $\mathcal{H}(\Phi)$ depends linearly on Φ (see e.g. Thiele *et al.* (2013) and Todorova (2013) for a somewhat different linear dependence of F on ϕ only). Therefore, we have

$$\mathcal{H}(\Phi) = \mathcal{H}_{ref}(1 + \tau\Phi), \tag{3.15}$$

so that F can be written as

$$F(h, \Gamma, \phi) = F(h, \Phi) = (1 + \tau\Phi)\hat{F}(h). \tag{3.16}$$

Regarding the h-dependence, we consider a power-law dependence of $\hat{F}$ on h, as

$$\hat{F}(h) = \frac{\zeta^{1-n}}{n-1} - \frac{\zeta^{1-m}}{m-1}, \quad \zeta = \frac{h}{h_*}, \tag{3.17}$$

where $h_* = h_e/\bar{h}_0$. Figure 2 illustrates the form of F for $(n, m) = (3, 2)$, the values successfully used to model single metal instabilities (Kondic *et al.* 2020). Here, h_e is the equilibrium thickness.

4. Linear stability analysis

Next, we linearize the formulation by considering perturbations of order $\epsilon(\ll 1)$ as

$$\boldsymbol{\Lambda} \approx \boldsymbol{\Lambda}_0 + \epsilon\boldsymbol{\Lambda}_1, \quad \boldsymbol{P} \approx \boldsymbol{P}_0 + \epsilon\boldsymbol{P}_1, \quad \boldsymbol{Q} \approx \boldsymbol{Q}_0 + \epsilon\boldsymbol{Q}_1, \quad \boldsymbol{M} \approx \boldsymbol{M}_0 + \epsilon\boldsymbol{M}_1, \quad \boldsymbol{J} \approx \boldsymbol{J}_0 + \epsilon\boldsymbol{J}_1. \tag{4.1a–e}$$

To the first order in ϵ, we obtain

$$\partial_t\boldsymbol{\Lambda}_1 - \boldsymbol{\nabla}\cdot(\boldsymbol{Q}_0\boldsymbol{\nabla}\boldsymbol{P}_1) = \boldsymbol{J}_1, \tag{4.2}$$

where

$$\begin{aligned}\boldsymbol{P}_1 &= \left.\frac{\partial\boldsymbol{P}}{\partial\boldsymbol{\Lambda}}\right|_{\boldsymbol{\Lambda}_0}\boldsymbol{\Lambda}_1 + \left.\frac{\partial\boldsymbol{P}}{\partial\boldsymbol{\Lambda}_x}\right|_{\boldsymbol{\Lambda}_0}\boldsymbol{\Lambda}_{1,x} + \left.\frac{\partial\boldsymbol{P}}{\partial\boldsymbol{\Lambda}_{xx}}\right|_{\boldsymbol{\Lambda}_0}\boldsymbol{\Lambda}_{1,xx},\\ &= \boldsymbol{E}_0\boldsymbol{\Lambda}_1 + \boldsymbol{E}_1\boldsymbol{\Lambda}_{1,x} + \boldsymbol{E}_2\boldsymbol{\Lambda}_{1,xx}.\end{aligned} \tag{4.3}$$

Here, we omit the y-dependence for brevity, since our focus is on the two-dimensional problem, i.e. we consider only an x-dependence. Note that we have $\boldsymbol{E}_1 = 0$, since all the gradients of Ψ in (2.18)–(2.20) are quadratic and the base state is uniform ($\boldsymbol{\nabla}\boldsymbol{\Lambda}|_0 = 0$).

The right-hand side of (4.2) is

$$\boldsymbol{J}_1 = -\boldsymbol{M}_0\boldsymbol{P}_1 - \boldsymbol{M}_1\boldsymbol{P}_0, \tag{4.4}$$

where

$$\boldsymbol{M}_1 = 3D_s\Gamma_1 \begin{pmatrix} 0 & 0 & 0 \\ 0 & 1/s & -1 \\ 0 & -1 & s \end{pmatrix}. \tag{4.5}$$

Note that the last term in (4.4) can be written as

$$\boldsymbol{M}_1\boldsymbol{P}_0 = 3D_s\left(\frac{\mu_{s,0}}{s} - \mu_0\right)\Gamma_1 \begin{pmatrix} 0 \\ 1 \\ -s \end{pmatrix} = 0. \tag{4.6}$$

Thus, this contribution to J_1 vanishes due to (3.3).

By considering a perturbation in terms of normal modes

$$\boldsymbol{\Lambda} = \boldsymbol{\Lambda}_0 + \epsilon \boldsymbol{X}\, \mathrm{e}^{\mathrm{i}kx+\omega t}, \tag{4.7}$$

then (4.2) leads to

$$\omega \boldsymbol{X} = [(k^2\boldsymbol{Q}_0 + \boldsymbol{M}_0)(k^2\boldsymbol{E}_2 - \boldsymbol{E}_0)]\boldsymbol{X}, \tag{4.8}$$

where ω and $\boldsymbol{X}$ are the eigenvalue and eigenfunction of the system.

As defined in (4.3), the matrix operator $\boldsymbol{E_0}$ of the linearized problem is given by

$$\boldsymbol{E}_0 = \begin{pmatrix} \left.\frac{\partial p}{\partial h}\right|_0 & \left.\frac{\partial p}{\partial \Gamma}\right|_0 & \left.\frac{\partial p}{\partial \psi}\right|_0 \\ \left.\frac{\partial \mu_s}{\partial h}\right|_0 & \left.\frac{\partial \mu_s}{\partial \Gamma}\right|_0 & \left.\frac{\partial \mu_s}{\partial \psi}\right|_0 \\ \left.\frac{\partial \mu}{\partial h}\right|_0 & \left.\frac{\partial \mu}{\partial \Gamma}\right|_0 & \left.\frac{\partial \mu}{\partial \psi}\right|_0 \end{pmatrix}, \quad \boldsymbol{E}_2 = \begin{pmatrix} \left.\frac{\partial p}{\partial h_{xx}}\right|_0 & \left.\frac{\partial p}{\partial \Gamma_{xx}}\right|_0 & \left.\frac{\partial p}{\partial \psi_{xx}}\right|_0 \\ \left.\frac{\partial \mu_s}{\partial h_{xx}}\right|_0 & \left.\frac{\partial \mu_s}{\partial \Gamma_{xx}}\right|_0 & \left.\frac{\partial \mu_s}{\partial \psi_{xx}}\right|_0 \\ \left.\frac{\partial \mu}{\partial h_{xx}}\right|_0 & \left.\frac{\partial \mu}{\partial \Gamma_{xx}}\right|_0 & \left.\frac{\partial \mu}{\partial \psi_{xx}}\right|_0 \end{pmatrix}, \tag{4.9a,b}$$

where p, μ_s and μ are given by (2.18)–(2.20). This calculation yields the matrices $\boldsymbol{E}_0$ and $\boldsymbol{E}_2$ as

$$\boldsymbol{E}_0 = K \begin{pmatrix} \phi_0(U\phi_0 - 2F^0_{h\phi} + 2F^0_{\phi}) + F^0_{hh} & F^0_{h\Gamma} - F^0_{\Gamma\phi}\phi_0 & F^0_{h\phi} - F^0_{\phi} - U\phi_0 \\ F^0_{h\Gamma} - F^0_{\Gamma\phi}\phi_0 & F^0_{\Gamma\Gamma} + \dfrac{\beta_s}{K}G^0_{s,\Gamma\Gamma} & F^0_{\Gamma\phi} \\ F^0_{h\phi} - F^0_{\phi} - U\phi_0 & F^0_{\Gamma\phi} & U \end{pmatrix}, \tag{4.10}$$

where $U = F^0_{\phi\phi} + \beta G^0_{\phi\phi}/K$, and

$$\boldsymbol{E}_2 = \begin{pmatrix} \Gamma_0(KF^0_{\Gamma} + \beta_s G^0_{s,\Gamma}) - \beta_s G^0_s - \Sigma\phi_0^2 & 0 & \Sigma\phi_0 \\ 0 & -s\Sigma & 0 \\ \Sigma\phi_0 & 0 & -\Sigma \end{pmatrix}. \tag{4.11}$$

Here, the subscripts on F, G and G_s stand for derivatives, and the superscript 0 indicates that they are evaluated at the base state $(1, \Gamma_0, \phi_0)$. Note that, as expected, both $\boldsymbol{E}_0$ and

$\boldsymbol{E}_2$ are symmetric matrices. Thus, the LSA for the normal modes finally leads to the eigenvalue problem (see (4.8))

$$\omega \boldsymbol{X} = \boldsymbol{A}\boldsymbol{X}, \tag{4.12}$$

where

$$\boldsymbol{A} = \boldsymbol{C}\boldsymbol{E}, \tag{4.13}$$

and

$$\boldsymbol{E} = k^2\boldsymbol{E}_2 - \boldsymbol{E}_0, \quad \boldsymbol{C} = k^2\boldsymbol{Q}_0 + \boldsymbol{M}_0, \tag{4.14a,b}$$

with

$$\boldsymbol{C} = \begin{pmatrix} k^2 & \dfrac{3k^2\Gamma_0}{2} & k^2\phi_0 \\ \dfrac{3k^2\Gamma_0}{2} & \left(3\Gamma_0^2 + \dfrac{3D\Gamma_0}{s}\right)k^2 + \dfrac{3D\Gamma_0}{s^2} & \dfrac{3}{2}k^2\Gamma_0\phi_0 - \dfrac{3D\Gamma_0}{s} \\ k^2\phi_0 & \dfrac{3}{2}k^2\Gamma_0\phi_0 - \dfrac{3D\Gamma_0}{s} & (\phi_0^2 + 3D\phi_0)k^2 + 3D\Gamma_0 \end{pmatrix}. \tag{4.15}$$

For reference, in Appendix A, we outline a proof showing that since $\boldsymbol{C}^{-1}$ is positive definite and $\boldsymbol{E}$ are symmetric, the eigenvalues of the matrix $\boldsymbol{A}$ are real. Therefore, the perturbations grow or decay exponentially in time.

The dispersion relation corresponding to (4.8) is obtained by requiring

$$\det[\omega\boldsymbol{I} - (k^2\boldsymbol{Q}_0 + \boldsymbol{M}_0)(k^2\boldsymbol{E}_2 - \boldsymbol{E}_0)] = 0. \tag{4.16}$$

The critical wavenumber k_c at which $\omega(k_c) = 0$ is obtained from

$$\det[k_c^2\boldsymbol{E}_2 - \boldsymbol{E}_0] = 0, \tag{4.17}$$

since $(k^2\boldsymbol{Q}_0 + \boldsymbol{M}_0)$ is positive definite. We note that the eigenvalue problem in (4.8) has two modes which have $\omega(k = 0) = 0$ (onset of the instability) since the three governing equations correspond to two conservation laws. The other real k_c values, when they exist, limit the band of unstable wavenumbers.

Finally, the above equation does not necessarily lead to $\omega = 0$ at $k = 0$ for all modes. In fact, (4.16) for $k = 0$ becomes

$$\det[\omega_0\boldsymbol{I} + \boldsymbol{M}_0\boldsymbol{E}_0] = 0, \tag{4.18}$$

where $\omega_0 = \omega(k = 0)$. Although $\omega_0 = 0$ is a possibility since $\det\boldsymbol{M}_0 = 0$, another root $\omega_0 \neq 0$ exists.

We proceed by discussing two separate sub-cases: (i) the pure Marangoni case, such that the fluid–solid interaction potential is concentration independent, and (ii) the general case, such that both the Marangoni effect and the influence of concentration-dependent wetting potentials isconsidered. The results are illustrated by analysing the instability of a metallic binary alloy.

5. Marangoni effect with wetting energy depending only on film thickness

When the wettability does not depend on the concentrations Γ and ϕ, i.e. $F = \hat{F}(h)$, the matrix $\boldsymbol{A}$, see (4.13), takes the form

$$\boldsymbol{A}_M = \begin{pmatrix} \tilde{\omega}_h & -\dfrac{3}{2}k^2\Gamma_0\Delta & 0 \\ \Gamma_0\left(\dfrac{3}{2}\tilde{\omega}_h + \dfrac{\tilde{\omega}_\psi}{sk^2}\right) & -\dfrac{3\Gamma_0\Delta[(1+k^2s)D_s + k^2s\Gamma_0]}{s} & -\dfrac{\Gamma_0\tilde{\omega}_\psi}{k^2s\phi_0} \\ \phi_0(\tilde{\omega}_h - \tilde{\omega}_\psi) - \dfrac{\Gamma_0\tilde{\omega}_\psi}{k^2} & \dfrac{3}{2}\Gamma_0\Delta(2D_s - k^2\phi_0) & \tilde{\omega}_\psi\left(1 + \dfrac{\Gamma_0}{k^2\phi_0}\right) \end{pmatrix}, \tag{5.1}$$

where we have used the reference frequencies

$$\tilde{\omega}_h = k^2(\tilde{k}_{c,h}^2 - k^2), \quad \tilde{\omega}_\psi = 3D_s\Sigma_s\phi_0k^2(\tilde{k}_{c,\psi}^2 - k^2), \tag{5.2a,b}$$

with the corresponding wavenumbers

$$\tilde{k}_{c,h} = \sqrt{-\frac{K\hat{F}^0_{hh}}{\hat{\gamma}_0}}, \quad \tilde{k}_{c,\psi} = \sqrt{-\frac{\beta_sG^0_{\phi\phi}}{\Sigma_s}}, \tag{5.3a,b}$$

and $\Delta = \Sigma_sk^2 + \beta_sG^0_{s,\Gamma\Gamma}$.

According to (4.17), the critical wavenumbers k_c, when they are real, that limit the band of unstable wavenumbers from above are

$$k_{c,1} = \tilde{k}_{c,h}, \quad k_{c,2} = \tilde{k}_{c,\psi}, \quad k_{c,3} = \sqrt{-\frac{\beta_sG^0_{s,\Gamma\Gamma}}{\Sigma_s}}. \tag{5.4a–c}$$

Thus, in order to have a real critical wavenumber, at least one of the second derivatives F^0_{hh}, $G^0_{\phi\phi}$ and $G^0_{s,\Gamma\Gamma}$ must be negative. Otherwise, no instability is possible. In fact, when using (3.17) for the wetting energy dependence on h, $\hat{F}(h)$, as well as (3.8) for G and (3.9) for G_s, we have

$$F^0_{hh} = \hat{F}^0_{hh} < 0, \quad G^0_{s,\Gamma\Gamma} = \frac{1}{\Gamma_0(1-\Gamma_0)} > 0, \quad G^0_{\phi\phi} = \frac{1}{\phi_0(1-\phi_0)} > 0, \tag{5.5a–c}$$

for $h > 1.5h_e$ (see figure 2). Thus, there is only one unstable mode, since only $k_{c,1}$ is real and positive. However, if an alternative expression for G, G_s (e.g. the double-well potential as in Diez *et al.* 2021) is used, another unstable mode may appear. Note that the critical wavenumbers reported in Diez *et al.* (2021) correspond to $k_{c,1}$ with $\hat{\gamma}_0 = 1$ (no Marangoni effect), and $k_{c,2}$. Therefore, the Marangoni effect increases the unstable k-range since it leads to a larger $\tilde{k}_{c,1}$ due to the decrease in $\hat{\gamma}_0$ with respect to the case without surfactant. However, if one compares a film with a homogeneous surfactant with another one without surfactant but with the same surface tension, there is no change in $k_{c,h}$.

The characteristic equation corresponding to $\boldsymbol{A}_M$ in (5.1) is given by

$$\begin{aligned} &6\Delta\Gamma_0^2s\tilde{\omega}_\psi[2D_s(\omega - \tilde{\omega}_h) + \tilde{\omega}_\psi(\phi_0k^2 + \Gamma_0) - \phi_0k^2\omega] \\ &\quad + \{4s\omega(\omega - \tilde{\omega}_h) + 12D_s(1+sk^2)\Delta\Gamma_0(\omega - \tilde{\omega}_h) + 3\Delta\,\Gamma_0^2[sk^2(4\omega - \tilde{\omega}_h) + 2\tilde{\omega}_\psi]\} \\ &\quad \times [\phi_0k^2(\omega - \tilde{\omega}_\psi) - \Gamma_0\tilde{\omega}_\psi] = 0. \end{aligned} \tag{5.6}$$

In what follows, we find it convenient to consider the case $s \ll 1$ (thin interface), since the leading-order results (found by considering the limit $s \to 0$) simplify considerably.

For the dispersion relation specified by (5.6), such a limit leads to

$$12D_s k^2 \Delta\Gamma_0 \phi_0 (\omega - \tilde{\omega}_h)(\omega - \tilde{\omega}_\psi) = 0, \tag{5.7}$$

which has the roots $(\tilde{\omega}_h, \tilde{\omega}_\psi)$. When comparing with the results obtained without consideration of the Marangoni effect, see Diez *et al.* (2021), we observe that they are functionally identical, except for the fact that the presence of the Marangoni effect modifies $\tilde{k}_{c,h}$. Since the maximum growth rates are proportional to $\tilde{k}_{c,h}^4$ and $\tilde{k}_{c,\psi}^4$, the increased $\tilde{k}_{c,h}$ also implies a larger maximum of $\tilde{\omega}_h$. Note that the modes $\tilde{\omega}_h$ and $\tilde{\omega}_\psi$ coincide (i.e. degenerate) at the wavenumber

$$k_d = \sqrt{\frac{\tilde{k}_{c,h}^2 + 3D\Sigma\phi_0 G^0_{\phi\phi}}{1 - 3D\Sigma\phi_0}}. \tag{5.8}$$

Since we here consider $G^0_{\phi\phi} > 0$ and relatively small values of $D\Sigma$, we can assure that this crossing point (where $\tilde{\omega}_h = \tilde{\omega}_\psi$) exists for all values of ϕ_0 and $k_d > \tilde{k}_{c,h}$.

Let us now analyse the main characteristics of matrix $\boldsymbol{A}_M$ in (5.1). For $k = 0$, we have (see also (4.18))

$$\boldsymbol{A}_M(k=0) = \frac{3D_s\Gamma_0\beta_s}{s}\begin{pmatrix} 0 & 0 & 0 \\ -\phi_0 G^0_{\phi\phi} & -G^0_{s,\Gamma\Gamma} & G^0_{\phi\phi} \\ s\phi_0 G^0_{\phi\phi} & sG^0_{s,\Gamma\Gamma} & -sG^0_{\phi\phi} \end{pmatrix}, \tag{5.9}$$

which has two vanishing eigenvalues, $\omega_1 = \omega_2 = 0$ (as expected due to the fact that there are two conserved quantities in the problem, h and ψ), as well as

$$\omega_3 = -3D_s\Gamma_0\beta_s\left(G^0_{\phi\phi} + \frac{G^0_{s,\Gamma\Gamma}}{s}\right), \tag{5.10}$$

whose eigenvector is $\boldsymbol{X}_3 = (0, -1/s, 1)$. Therefore, this mode only affects Γ and ψ, and it does not contribute to h, i.e. to the film stability. It represents a spatially uniform decrease of Γ while ϕ increases ($\boldsymbol{J}_1 \neq 0$). When both $G^0_{s,\Gamma\Gamma}$ and $G^0_{\phi\phi}$ are positive, this concentration mode is stable, confirming the thermodynamic consistency.

Regarding the behaviour of ω as $k \to \infty$, we note the matrix $\boldsymbol{A}$ in (5.1) adopts the form

$$\boldsymbol{A}_M(k\to\infty) = k^4\begin{pmatrix} -\hat{\gamma}_0 & -\frac{3}{2}\Sigma_s\Gamma_0 & 0 \\ -\frac{3}{2}\Gamma_0\hat{\gamma}_0 & -3\Sigma_s\Gamma_0(D_s+\Gamma_0) & 0 \\ \phi_0(3D_s\Sigma_s\phi_0 - \hat{\gamma}_0) & -\frac{3}{2}\Sigma_s\Gamma_0\phi_0 & -3D_s\Sigma_s\phi_0 \end{pmatrix}. \tag{5.11}$$

Note that $\hat{\gamma}_0$ is the surface tension of the base state $\boldsymbol{\Lambda} = (1, \Gamma_0, \psi_0)$. Considering the structure of the third column of the matrix defined by (5.11), we immediately realize that one eigenvalue is $\omega_3^\infty = -3D_s\Sigma_s\phi_0 k^4 < 0$, so that this mode is stable. In order to find the sign of ω_1^∞ and ω_2^∞, we analyse their characteristic quadratic equations as given by the elements of the submatrix formed by the first two elements of the first and second rows.

Parameter	Value	Constant	Value
ϕ_0	0.4	(n, m)	(3, 2)
T	2200	K	1.081
$\bar{h}_0$	15 nm	β	0.4643
h_e	1 nm	β_s	0.03095
a	1 nm	Σ	1.39×10^{-4}
a_s	1 nm	Σ_s	9.25×10^{-6}
η	2 mPa s	D	1.83×10^{-3}
$\mathcal{H}_{ref}$	2×10^{-17} J	D_s	2.74×10^{-2}
γ_{ref}	0.981 J m^{-2}	s	0.067
σ	1.816×10^{-10} J m^{-2}	h_*	0.067

Table 2. List of dimensional parameters and non-dimensional constants that characterize the experimental set-up.

We find that their sum and product are given by

$$\omega_1^\infty + \omega_2^\infty = -\hat{\gamma}_0 k^4 - 3\Sigma_s \Gamma_0 (D_s + \Gamma_0) k^4, \quad \omega_1^\infty \omega_2^\infty = \frac{3}{4} \Gamma_0 \Sigma_s (4D_s + \Gamma_0) \hat{\gamma}_0 k^8. \tag{5.12a,b}$$

Since the product is positive and the sum is negative, both modes are stable for $k \to \infty$, as expected.

5.1. *Linear stability analysis results: eigenvalues and eigenfunctions*

In the following, we apply the formulation to alloys of nanometric thickness melted by laser radiation. The experiments reported in Diez *et al.* (2021) correspond to a binary system such that fluids A and B are silver, Ag, and nickel, Ni, respectively. The results have shown that the films become unstable and break up into drops, which typically consist of both metals. In the context of modelling results, we use the expression 'breakup' to signify film thickness reaching its equilibrium, h_e, discussed later in this section. In that work, the instability leading to breakup was analysed based only on two fields, h and ψ, without Marangoni effects. The growth rates obtained were $\tilde{\omega}_h$ with $\hat{\gamma}_0 = 1$ and $\tilde{\omega}_\psi$. Here, we discuss the modifications of the results due to the influence of the Marangoni effect and the presence of the additional field, Γ.

We consider the specific alloy $Ag_{40}Ni_{60}$, so that we have $\phi_0 = 0.4$ as the initial concentration of the A-component. The appropriate choice of material parameters for the problem of alloys (binary fluid) was also discussed in Diez *et al.* (2021), where we considered non-constant temperature of the alloy due to heating and cooling by a laser. In the present work, for simplicity, we do not consider thermal aspects of the problem.

The first two columns of table 2 give the values of the parameters, while the third and fourth columns show the corresponding non-dimensional constants. The resulting time scale, see (2.8), is $t_c = 180.47$ ns, where we have used a spatial scale $\ell = 100$ nm.

Figure 3 shows by solid lines the dispersion curves $\omega(k)$ for the metal alloy when the Marangoni effect is included, but the wetting energy depends on h only, i.e. the eigenvalues of $\boldsymbol{A}_M$. The dashed lines correspond to the solutions for $s \to 0$ given by (5.7). Note that the maximum growth rate, ω_m, is only slightly smaller than the one obtained by considering $s \to 0$ (dashed lines), as expected, since s is fairly small (see table 2). Note that, around the crossing point of the dashed lines ($k \approx k_d$), the degeneracy of the modes $\tilde{\omega}_h$ and $\tilde{\omega}_\psi$ is

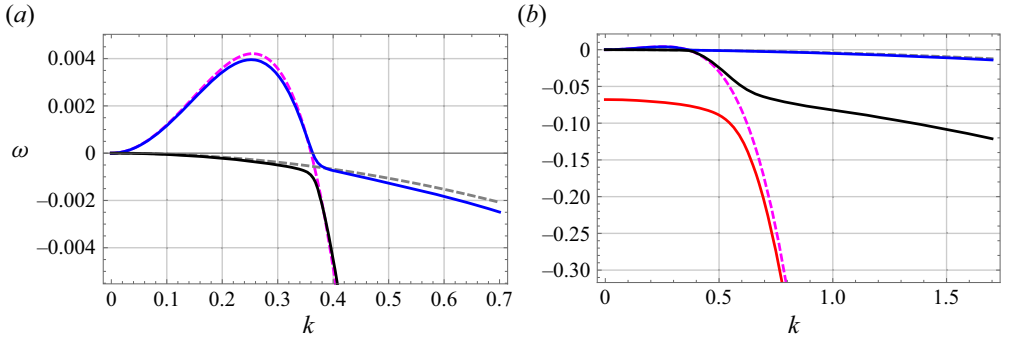

Figure 3. Dispersion relations including Marangoni effect and considering wetting energy depending only on thickness ($\tau = 0$): (a) zooms into the unstable region (small k values), and (b) shows the results for a larger k-range. The solid blue, black and red lines show $\omega_{1,2,3}(k)$, while the dashed lines correspond to the results for $s \to 0$, $\tilde{\omega}_h$ (magenta) and $\tilde{\omega}_\psi$ (grey).

broken for $s > 0$ (see figure 3a). Therefore, the mode 1 (blue line), which for $k < k_d$ can be associated with $\tilde{\omega}_h$ (magenta dashed line), i.e. the h unstable mode, converts for $k > k_d$ into a mode dominated by the ψ-evolution associated with $\tilde{\omega}_\psi$ (black dashed line). The reverse occurs for mode 2. However, for sufficiently large k, mode 1 departs from both $\tilde{\omega}_h$ and $\tilde{\omega}_\psi$, while mode 3 (solid red line in figure 3b) approaches the asymptotic behaviour of $\tilde{\omega}_h$.

Once the eigenvalues $\omega_i(k)$ $(i = 1, 2, 3)$ are obtained, we proceed to calculate the corresponding complex amplitudes of the eigenfunctions

$$\boldsymbol{X}_i = \begin{pmatrix} h_{1i} \\ \Gamma_{1i} \\ \psi_{1i} \end{pmatrix}, \tag{5.13}$$

for each normal mode at a given k (see (4.8)), and $|\boldsymbol{X}_i|^2 = h_{1i}^2 + \Gamma_{1i}^2 + \psi_{1i}^2 = 1$. Note that, due to the nature of the considered problem, all the amplitudes are, in fact, real numbers with their signs indicating whether Γ_{1i} or ψ_{1i} are in-phase or anti-phase with h_{1i}. Figure 4 shows the eigenfunctions corresponding to the eigenvalues $\omega_{1,2,3}(k)$ in figure 3. For $k < k_d = 0.3689$, figure 4(a) shows that the amplitude of the h-eigenfunctions of mode 3 are negligible with respect to those of modes 1 and 2. Instead, in the same k-range, figure 4(b) shows that the amplitude of the unstable mode 1 for Γ is very small, while those of modes 2 and 3 are much larger. Finally, figure 4(c) shows that the amplitude of the ψ-eigenfunction is negligible for mode 3 in comparison with modes 1 and 2. These results illustrate that, for the unstable k range, modes 1 and 2 are mainly connected with perturbations in h and ψ, respectively, while mode 3 is more prone to be excited by perturbations in Γ. These results are in agreement with the previous discussion on the conversion of modes when degeneracy close to k_d is broken for $s > 0$. Also, note that the transitions between in-phase and anti-phase behaviour of the Γ_{11} and ψ_{13} modes occur at k_d.

5.2. *Nonlinear regime*

We proceed by solving numerically the nonlinear (2.11a)–(2.11c); see Appendix B for details. We consider the initial condition corresponding to the monochromatic

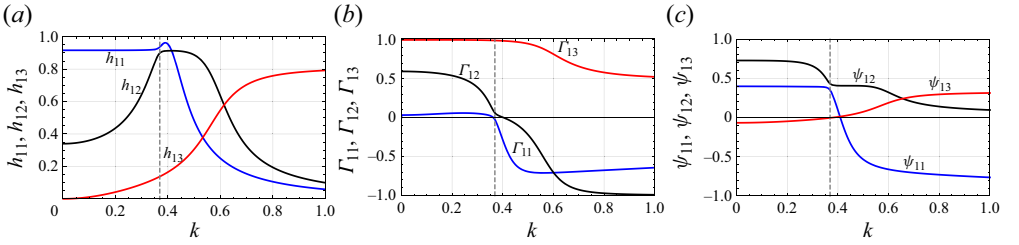

Figure 4. Amplitudes of the eigenfunctions including Marangoni effect and considering wetting energy depending only on thickness ($\tau = 0$) (dispersion relation shown in figure 3) for (*a*) h, (*b*) Γ and (*c*) ψ. The vertical grey dashed lines indicate the value of k_d.

perturbations of the three fields

$$\boldsymbol{\Lambda} = \boldsymbol{\Lambda}_0 + \epsilon_1 \boldsymbol{X}_1(k)\, \mathrm{e}^{\mathrm{i}kx+\omega_1(k)t}, \tag{5.14}$$

where $0 < \epsilon_1 \ll 1$. Here, we use $\epsilon_1 = 0.01$.

More precisely, we consider a flat uniform film in a spatial domain $0 \le x \le \lambda = 2\pi/k$ with periodic boundary conditions and initial perturbations as given by (5.14). We take $k = 0.25$, so that the corresponding eigenvalue is $\omega_1 = 0.00395$ (see figure 3). Figure 5(*a*) shows the corresponding h, Γ, ψ and ϕ profiles at different times. We observe the instability development until the film breakup and drop formation. Figure 6 compares the evolution of the perturbations at $x = 0$ with the LSA prediction, that is, an exponential growth with the corresponding eigenvalue, ω_1. Interestingly, the exponential growth is valid not only for small perturbations and early times (as expected), but even up to times close to the film breakup (i.e. h approaching h_*), when the perturbations have increased at least an order of magnitude with respect to their initial values. This result is consistent with similar ones found for other single-phase films, see, e.g. Sharma & Jameel (1993) and Sharma *et al.* (1995). The departure from the linear model is due to the change of the profiles with respect to the sinusoidal shape as the system approaches the breakup (see figure 3*c*,*d*), which requires the excitation of new wavenumbers because of a nonlinear transfer of energy to these new k values (see figure 6(*a*) for $t > 1000$). As a consequence, the evolution of the perturbations with the original wavenumber tends to a plateau, since its energy is depleted to feed the other wavenumbers. Note that ϕ and Γ become identical for very long times, i.e. when the drop has formed since it constitutes a new equilibrium state.

Moreover, the LSA can be used to estimate the breakup time as

$$t_{break} = \frac{1}{\omega_1} \ln \frac{1 - h_*}{\epsilon_1}, \tag{5.15}$$

which yields $t_{break} = 1184$. According to the numerical simulations, this time should be between those shown in figure 5*c*,*d*) (i.e. between $t = 953$ and 1108), so that the prediction from LSA gives a reasonable estimate.

Next, we consider the case when all three normal modes are excited

$$\boldsymbol{\Lambda} = \boldsymbol{\Lambda}_0 + \epsilon_1 \boldsymbol{X}_1(k)\, \mathrm{e}^{\mathrm{i}kx+\omega_1(k)t} + \epsilon_2 \boldsymbol{X}_2(k)\, \mathrm{e}^{\mathrm{i}kx+\omega_2(k)t} + \epsilon_3 \boldsymbol{X}_3(k)\, \mathrm{e}^{\mathrm{i}kx+\omega_3(k)t}, \tag{5.16}$$

where ϵ_1, ϵ_2 and ϵ_3 were chosen so as to ensure that the amplitudes of the perturbations in h, Γ and ψ are initially equal to 0.01. Figure 6(*b*) compares the results of this numerical simulation (solid lines) with those of the LSA (dashed lines). We observe that the full

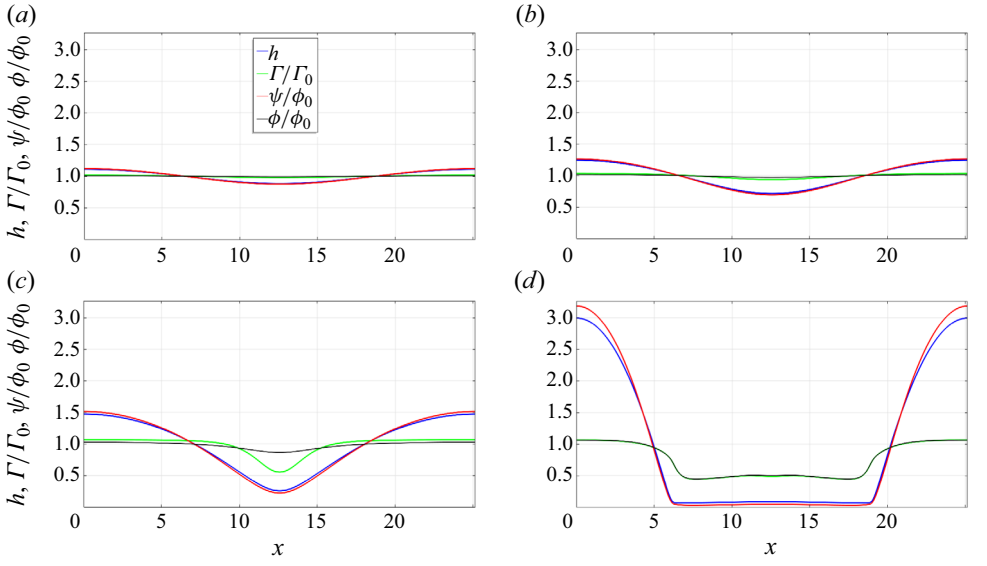

Figure 5. Spatial profiles of h, Γ, ψ and ϕ at different times obtained from the numerical solution of the nonlinear equations when the flat film is perturbed as in (5.14) with $k = 0.25$ only by mode 1 (with Marangoni effect and wetting energy depending only on thickness ($\tau = 0$)). Panels show (*a*) $t = 609$, (*b*) $t = 809$, (*c*) $t = 953$ and (*d*) $t = 1108$.

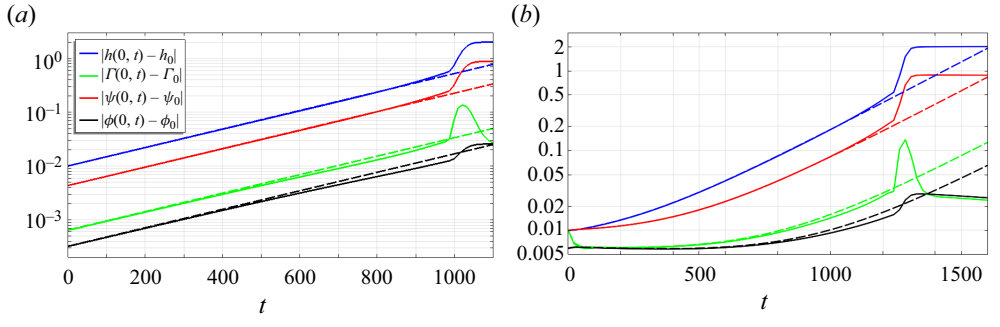

Figure 6. Perturbations at $x = 0$ as a function of time for a monochromatic ($k = 0.25$) perturbation including Marangoni effect and considering wetting energy depending only on thickness ($\tau = 0$). Dashed lines correspond to LSA for h (blue), Γ (green), ψ (red) and ϕ (black): (*a*) single unstable mode (see (5.14)), (*b*) all three modes (see (5.16)). Solid lines show the numerical simulation results with the same initial conditions.

problem is also very well described by the LSA, even up to times very close to breakup. Naturally, the evolution is not represented by a straight line (in linear–log scale), since it is a linear combination of three exponential terms.

Before concluding this section, we note that we have also considered a single mode perturbed by a superposition of two wavenumbers, one unstable and one stable (figures not shown for brevity). As expected, the stable wavenumber decays exponentially, while the unstable one grows. In the context of melted metallic thin films, if the duration of the laser pulses (and correspondingly the liquid lifetime) is shorter than the decay time, the subsequent solidification freezes the evolution. Therefore, the stable modes may still appear as an outcome of such experiments.

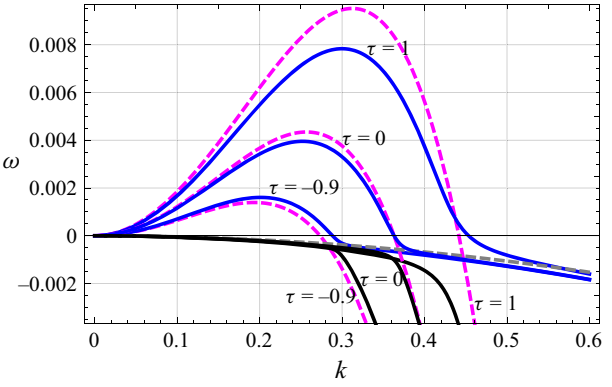

Figure 7. Dispersion relations for modes 1 (solid blue) and 2 (solid black) when both Marangoni effect and concentration-dependent wetting energy are considered ($\tau = 1$ and $\tau = -0.9$) compared with the case when the wetting energy depends only on h ($\tau = 0$) (also shown in figure 3). The magenta dashed lines correspond to $\tilde{\omega}_h$ and the grey dashed line corresponds to $\tilde{\omega}_\psi$.

6. Marangoni effect combined with concentration-dependent wetting energy

Let us now consider the wetting energy, F, that depends on both Γ and ϕ (see (3.16)). This type of dependence yields an additional contribution to matrix $\boldsymbol{A}$, see (4.13), of the form

$$\boldsymbol{A} = \boldsymbol{A}_M + k^2\boldsymbol{A}_1 + k^4\boldsymbol{A}_2, \tag{6.1}$$

where

$$\boldsymbol{A}_1 = \frac{\tau K}{2}(\hat{F}^0 - \hat{F}'^0)\begin{pmatrix} 3\Gamma_0 s - 2\phi_0 & 2s & 2 \\ 3\Gamma_0(2D + 2\Gamma_0 s - \phi_0) & 3\Gamma_0 s & 3\Gamma_0 \\ \phi_0(6D + 3\Gamma_0 s - 2\phi_0) & 2s\phi_0 & 2\phi_0 \end{pmatrix}, \tag{6.2}$$

$$\boldsymbol{A_2} = \frac{\tau K}{2} s\Gamma_0 \hat{F}^0 \begin{pmatrix} 2 & 0 & 0 \\ 3\Gamma_0 & 0 & 0 \\ 2\phi_0 & 0 & 0 \end{pmatrix}. \tag{6.3}$$

The additional contributions yield the characteristic equation which generalizes (5.6). Since the equation is rather cumbersome to deal with, we show here just the figures that use the parameters from the melted metal problem. The wetting energy dependence on concentration, i.e. $F(h, \Gamma, \phi)$, is assumed to be given by (3.13).

Let us first consider the case $s \to 0$. For a given τ, one solution is $\tilde{\omega}_h$ from (5.2*a*,*b*). In this expression, $\tilde{k}_{c,h}$ is calculated using F^0_{hh} (which depends linearly on τ), but $\hat{\gamma}_0 = 1$ (see (3.10)), since $\tilde{\omega}_h$ does not include Marangoni effect. Figure 7 represents these solutions for different values of τ as magenta dashed lines. In this figure, the grey dashed line corresponds to $\tilde{\omega}_\psi$, which is neither affected by the Marangoni effect, nor by the value of τ. Note that the crossings, where there is degeneracy of $\tilde{\omega}_h(\tau)$ and $\tilde{\omega}_\psi$, give new values of k_d that depend on τ.

Figure 7 also shows the corresponding dispersion relations for modes 1 (blue) and 2 (black) for $\tau = 1$ and for $\tau = -0.9$. These results show that the inclusion of the wetting energy dependence on concentrations ($\tau \neq 0$) produces significant changes of the growth rates with respect to $\tau = 0$. In particular, we observe that both the critical

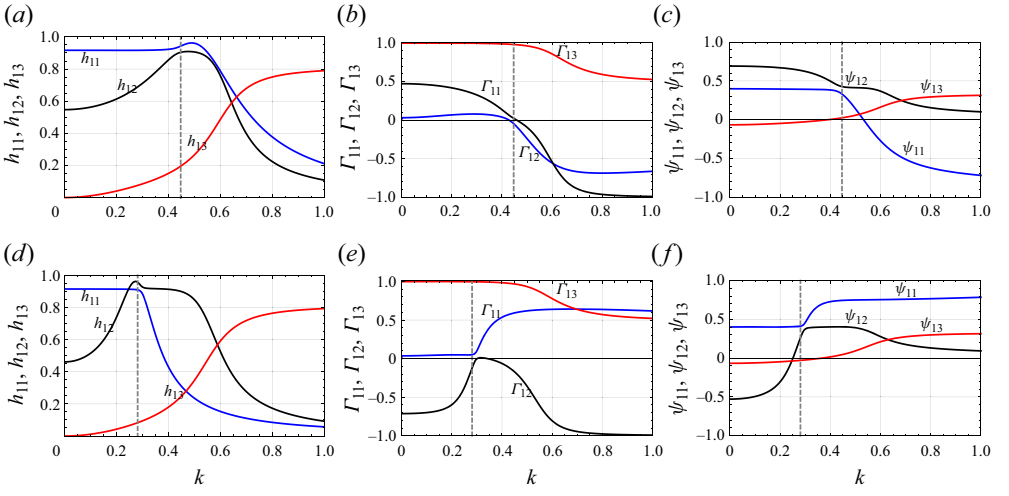

Figure 8. Amplitudes of eigenfunctions when both Marangoni effect and concentration-dependent wetting energy are considered for $\tau = 1.0$ (*a–c*) and $\tau = -0.9$ (*d–f*), and for (*a,d*) h, (*b,e*) Γ and (*c,f*) ψ. The vertical grey dashed lines indicate the value of k_d.

wavenumber, $k_{c,1}$, and the maximum growth rate, ω_m, increase (decrease) significantly for positive (negative) values of τ. As a consequence, the wavenumber of the maximum growth rate, k_m, can fall in the stable range of the $\tau = 0$ case for τ sufficiently large. The physical basis for this behaviour is that $\tau > 0$ increases the wetting energy, leading to increased instability of mode 1, which is dominated by the film thickness evolution. Note that the stable mode 3 is not shown in figure 7 since it corresponds to much smaller growth rates (see figure 3); the effect of τ is similar to what is shown in figure 7 for mode 2.

Figure 8 shows the amplitudes of the eigenfunctions for the eigenvalues shown in figure 7 for $\tau = 1$ and $\tau = -0.9$. We note that the amplitudes for $\tau = 0$ in figure 4 are qualitatively similar to the ones for $\tau = 1$ in figure 8, but the transitions between in-phase and anti-phase behaviour of the Γ_{11} and ψ_{13} modes move now to larger k values in consonance with the increase of $k_d (\approx k_c)$. However, there are remarkable differences between $\tau = 1$ and $\tau = -0.9$ in Γ and ψ for modes 1 and 2 . In fact, the comparison of Γ_{12} and ψ_{12} between both values of τ shows that they change sign for small k values (that include the unstable region of mode 1), while for large k values (stable region) this sign reversal does not occur. In contrast, there is no such sign change of Γ_{11} and ψ_{11} for small k values, but there is a sign change for large k values. Note that mode 3 is the least affected by the value of τ. As mentioned above, the contribution of h perturbations to mode 1 is predominant in the unstable domain (small k values), as seen by comparing the blue lines with the black and red ones in figure 8(*a,d*).

Figure 9 compares LSA predictions with the nonlinear numerical simulations for the considered values of τ. Here, we perturb the base state by a mode 1 monochromatic perturbation for $\tau = 1$ and $\tau = -0.9$ using $k = 0.2$. According to figure 7, this wavenumber corresponds to unstable perturbations. The comparison between figures 6(*a*), 9 (*a*) and 9(*c*) shows a similar qualitative behaviour, except for the fact that the time scales of the breakups change due to the different growth rates as τ varies (see figure 7). Clearly, the predictions of the LSA remain valid close to the breakup time, which varies as the inverse of the growth rate, ω_1.

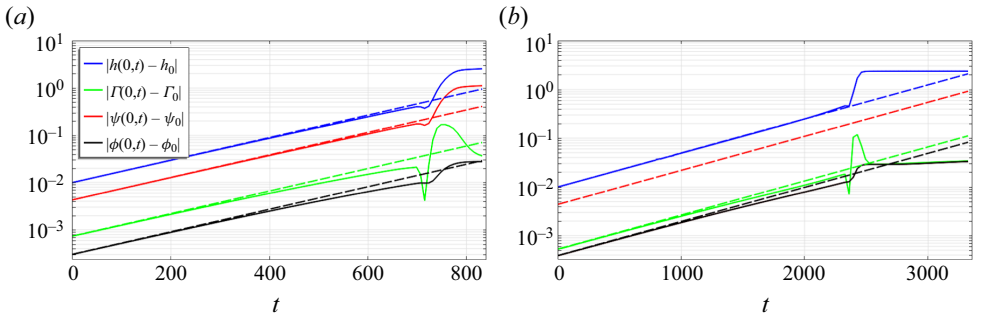

Figure 9. Perturbations at $x = 0$ as a function of time for mode 1 and $k = 0.2$ when both Marangoni effect and concentration-dependent wetting energy are considered. Solid lines: h (blue), Γ (green), ψ (red) and ϕ (black) as given by the numerical simulations for (*a*) $\tau = 1$ and (*b*) $\tau = -0.9$. Dashed lines: the LSA predictions. Note different time ranges for (*a*,*b*).

7. Summary and conclusions

This paper analyses the stability properties of a binary fluid thin film, focusing on the influence of the solutal Marangoni effects and the fluid–solid interaction, including its dependence on concentrations. The results include a LSA using analytical methods as well as a comparison with the numerical solutions of the full nonlinear problem. Due to the complexity of the task at hand, we have implemented various simplifications and attempted to concentrate on the main aspects of the problem as much as possible.

Carrying out tractable and insightful LSA requires the existence of a stationary base state. We find that such a state is possible when surface and volumetric chemical potentials are balanced, leading to vanishing (to the leading order) fluid exchange between the surface and the volume.

We find it helpful to separate the discussion into two separate cases. The first one focuses on the Marangoni effect assuming a wetting energy $F = F(h)$ (therefore concentration independent). Our finding is that the Marangoni effect alters the critical wavenumber, increasing the unstable k-range with respect to the results that do not include Marangoni effects (Diez *et al.* 2021). Therefore, the Marangoni effect leads to faster formation of smaller droplets, assuming that the LSA findings extend qualitatively to the nonlinear regime. We note that the previous experiments involving liquid metal nanometric films involve a set of parameters that allow for modelling of the problem accurately by assuming a very thin adsorption interface, which corresponds to the limit $s \to 0$ ($a_s \ll h_0$), and leads to simple analytical expressions for the growth rates. In the context of flows such that surfactants are relevant, we note that a case with surfactant and a certain surface tension compared with another without surfactant and the same surface tension (red dashed line in figure 3*a*) shows no change in $k_{c,h}$, but a slight decrease of the maximum growth rate.

Notably, comparing the LSA results with the numerical simulations of the full nonlinear problem reveals that most of the evolution is well described by the LSA results, with a significant difference between LSA and nonlinear simulations only very close to the film breakup time. Consequently, the validity of the linear approach can be extended to rather large unstable perturbations, confirming the LSA predictions regarding the expected size of the resulting drops and their formation times. We have made this comparison not only for single mode and monochromatic perturbations but also for a combination of modes and multiple wavenumbers. These combinations, which require a precise understanding of the stable modes, are relevant for the transient initial stages of the instability. In fact, this

transient behaviour may be of particular interest in the case of melted metallic films, since they could re-solidify and freeze the evolution before reaching the long-time asymptotic behaviour dominated by the unstable mode.

When additional dependence of the wetting energy on both surface and bulk concentrations is considered, we can describe its influence in terms of a single parameter, τ. As τ increases, both the critical wavenumber and the maximum growth rate of the unstable mode increase. While the Marangoni effect is found to be always destabilizing, the influence of concentration dependence of the wetting energy on concentrations could be either stabilizing ($\tau < 0$) or destabilizing ($\tau > 0$), compared with the $\tau = 0$ case. Therefore, the manner in which instability develops depends on the material properties of the considered fluids. For the considered case (including the wetting energy dependence on concentration), we have also confirmed an excellent agreement of the LSA results with the nonlinear numerical simulations until times close to film breakup.

Several aspects deserve future study. In this paper, we have selected particular forms of $G(\phi)$ and $G_s(\Gamma)$ that preclude the existence of additional unstable modes, since both are convex functions of their argument. However, one could also consider potentials that include concavity due to additional quadratic terms to an entropic or double-well potential. This could lead to new unstable modes with much larger growth rates (at also much larger wavenumber), as considered in Diez *et al.* (2021) for the case without the Marangoni effect and without consideration of concentration-dependent wetting energies, but with double-well potential. Therefore, an interesting extension of our analysis could be the inclusion of these types of potentials. A more involved aspect of the problem is the possibility that the base state is non-stationary, which occurs when the flux $\boldsymbol{J_0} \neq 0$. Considering these issues may allow for a better understanding of some features of experimentally observed results, such as core–shell and Janus-like droplets in the experiments carried out with liquid metals. We expect that our work provides a basic set-up that can serve as a basis for such endeavours.

Acknowledgements. The authors thank R. Allaire, L. Cummings and P. Rack for fruitful discussions.

Funding. This research was supported by NSF DMS-1815613 (L.K.), NSF CBET-1604351 (L.K., J.A.D., A.G.G.), ACS-PRF 62062-ND9 (L.K.), BSF 2020174 (L.K., J.A.D.) and NJIT faculty seed funding (L.K., J.A.D.). J.A.D and A.G.G. acknowledge support from Consejo Nacional de Investigaciones Científicas y Técnicas (CONICET, Argentina) with Grant PIP 02114-CO/2021 and Agencia Nacional de Promoción Científica y Tecnológica (ANPCyT, Argentina) with Grant PICT 02119/2020.

Declaration of interest. The authors report no conflict of interest.

Author ORCIDs.
J.A. Diez https://orcid.org/0000-0001-7751-5350;
A.G. González https://orcid.org/0000-0002-4710-6414;
L. Kondic https://orcid.org/0000-0001-6966-9851.

Appendix A. Discussion of the eigenvalue properties

We consider here the eigenvalues of (4.12). For the purpose of understanding their properties, we consider the generalized eigenvalue problem (Parlett 1998) by multiplying the equation by the inverse matrix $\boldsymbol{C}^{-1}$, if $\boldsymbol{C}$ is not singular

$$\omega \boldsymbol{C}^{-1}\boldsymbol{X} = \boldsymbol{E}\boldsymbol{X}. \tag{A1}$$

This can be done since $\boldsymbol{C}^{-1}$ is positive definite. In fact, a necessary and sufficient condition for the real symmetric matrix $\boldsymbol{C}^{-1}$ to be positive definite is that all the upper

left submatrices C_k^{-1} have positive determinants (Strang 1988). These are given by

$$S_1 \equiv C_{11}^{-1} = \frac{1}{h^3\Delta}[4D_s(3D\psi(\Gamma + k^2 s) + h(\Gamma\psi^2 + s\psi(3\Gamma^2 + k^2\psi) + 3\Gamma^3 s^2)) + \Gamma h k^2 s\psi(12D + h\psi) + 12\Gamma^2 D_s^2 s^2], \tag{A2}$$

$$S_2 \equiv \begin{vmatrix} C_{11}^{-1} & C_{12}^{-1} \\ C_{21}^{-1} & C_{22}^{-1} \end{vmatrix} = \frac{1}{h^3\Delta}\frac{4s(k^2\psi(3D + h\psi) + 3\Gamma^2 D_s s)}{3\Gamma k^2}, \tag{A3}$$

$$S_3 \equiv \det(C^{-1}) = \frac{4s}{3h^3\Delta}, \tag{A4}$$

where

$$\Delta = 3k^2(4DD_s\psi(\Gamma + k^2 s) + \Gamma D h k^2 s\psi + 4\Gamma^2 D_s^2 s^2 + \Gamma^3 D_s h s^2). \tag{A5}$$

Clearly, all determinants are positive since all variables and parameters are.

Since $\boldsymbol{C}^{-1}$ is positive definite, it can be decomposed by the Cholesky factorization

$$\boldsymbol{C}^{-1} = \boldsymbol{L}\boldsymbol{L}^\top, \tag{A6}$$

where $\boldsymbol{L}$ is a lower triangular matrix with real coefficients. Then, (A1) can be written as (Peters & Wilkinson 1970)

$$\left.\begin{array}{c} \omega\boldsymbol{L}\boldsymbol{L}^\top\boldsymbol{X} = \boldsymbol{E}\boldsymbol{X} \\ \boldsymbol{L}^{-1}(\omega\boldsymbol{L}\boldsymbol{L}^\top\boldsymbol{X}) = \boldsymbol{L}^{-1}(\boldsymbol{E}\boldsymbol{X}) \\ \omega\boldsymbol{L}^\top\boldsymbol{X} = \boldsymbol{L}^{-1}\boldsymbol{E}\boldsymbol{X} \\ \omega\boldsymbol{L}^\top\boldsymbol{X} = \boldsymbol{L}^{-1}\boldsymbol{E}\boldsymbol{L}^{-\top}\boldsymbol{L}^\top\boldsymbol{X} \end{array}\right\}. \tag{A7}$$

If $\boldsymbol{Y} = \boldsymbol{L}^\top\boldsymbol{X}$, we can write the standard eigenvalue problem

$$\omega\boldsymbol{Y} = (\boldsymbol{L}^{-1}\boldsymbol{E}\boldsymbol{L}^{-\top})\boldsymbol{Y} \equiv \boldsymbol{B}\boldsymbol{Y}. \tag{A8}$$

Note that matrix $\boldsymbol{B}$ satisfies the relation

$$\boldsymbol{B}^\top = ((\boldsymbol{L}^{-1}\boldsymbol{E})\boldsymbol{L}^{-\top})^\top = \boldsymbol{L}^{-1}(\boldsymbol{L}^{-1}\boldsymbol{E})^\top = \boldsymbol{L}^{-1}\boldsymbol{E}\boldsymbol{L}^{-\top} = \boldsymbol{B}, \tag{A9}$$

since $\boldsymbol{E}$ is symmetric. Therefore, $\boldsymbol{B}$ is also symmetric, and consequently, we claim that (A8) has real eigenvalues, ω. In order to prove this statement, let us now take the complex conjugate of (A8)

$$\omega^*\boldsymbol{Y}^* = \boldsymbol{B}\boldsymbol{Y}^*, \tag{A10}$$

where $\boldsymbol{B}$ is a real matrix. By multiplying (A8) by $\boldsymbol{Y}^*$ and (A10) by $\boldsymbol{Y}$, and subtracting both equations, we have

$$(\omega - \omega^*)|\boldsymbol{Y}|^2 = \boldsymbol{Y}^*\boldsymbol{B}\boldsymbol{Y} - \boldsymbol{Y}\boldsymbol{B}\boldsymbol{Y}^* = 0, \tag{A11}$$

since

$$\boldsymbol{Y}\boldsymbol{B}\boldsymbol{Y}^* = \boldsymbol{Y}^*(\boldsymbol{Y}\boldsymbol{B}) = \boldsymbol{Y}^*\boldsymbol{B}^\top\boldsymbol{Y} = \boldsymbol{Y}^*\boldsymbol{B}\boldsymbol{Y}, \tag{A12}$$

because $\boldsymbol{B} = \boldsymbol{B}^\top$. Consequently, ω is real.

Appendix B. Numerical simulations

The form of (2.11*a*)–(2.11*c*) is convenient to treat with the COMSOL Multiphysics formulation of partial differential equation coefficients form. This package solves by finite elements a vectorial equation for the unknown vector $\boldsymbol{u} = (u_1, u_2, \ldots, u_N)^\top$, which reads as

$$\boldsymbol{e}\frac{\partial^2 \boldsymbol{u}}{\partial t^2} + \boldsymbol{d}\frac{\partial \boldsymbol{u}}{\partial t} + \boldsymbol{\nabla}\cdot(-\boldsymbol{c}\boldsymbol{\nabla}\boldsymbol{u} - \boldsymbol{\alpha}\boldsymbol{u} + \boldsymbol{\gamma}) + \boldsymbol{\beta}\boldsymbol{\nabla}\boldsymbol{u} + \boldsymbol{a}\boldsymbol{u} = \boldsymbol{f}, \tag{B1}$$

where the coefficients of the N scalar equations are in the matrices $\boldsymbol{e}, \boldsymbol{d}, \boldsymbol{\gamma}, \boldsymbol{a}$ (of dimensions $N \times N$), $\boldsymbol{\alpha}, \boldsymbol{\beta}$ (of dimensions $N \times N \times n$), $\boldsymbol{c}$ (of dimensions $N \times N \times n \times n$) and the vector $\boldsymbol{f}$ (of dimension N), where n is the spatial dimension of the problem ($n = 1, 2, 3$). In index notation, this expression reads as

$$e_{ij}\frac{\partial^2 u_j}{\partial t^2} + d_{ij}\frac{\partial u_j}{\partial t} + \frac{\partial}{\partial x_l}\left(-c_{ijkl}\frac{\partial u_j}{\partial x_k} - \alpha_{ijl}u_j + \gamma_{il}\right) + \beta_{ijl}\frac{\partial u_j}{\partial x_l} + a_{ij}u_j = f_i, \tag{B2}$$

where $i, j = 1 \ldots, N$ and $k, l = 1, \ldots, n$.

In our system of equations, we define six components $u = (h, \Gamma, \psi, p, \mu_s, \mu)$ ($N = 6$) and we use six equations, namely, (2.11*a*)–(2.11*c*) and (2.18)–(2.20) for a one-dimensional problem ($n = 1$).

Below, we list the coefficients which are not zero for our system (since $k = l = 1$, we omit these indexes for brevity and consider $x_1 \equiv x$).

(a) Row 1 ($i = 1$) for (2.11*a*)

$$d_{11} = 1, \quad c_{14} = h^3, \quad c_{15} = \tfrac{3}{2}h^2\Gamma, \quad c_{16} = h^2\psi. \tag{B3a–d}$$

(b) Row 2 ($i = 2$) for (2.11*b*)

$$d_{22} = 1, \quad c_{24} = \tfrac{3}{2}h^2\Gamma, \quad c_{25} = 3h\Gamma^2 + 3D_s\Gamma, \quad c_{26} = \tfrac{3}{2}h\psi\Gamma, \tag{B4a–d}$$

$$a_{25} = 3D_s\Gamma/s, \quad a_{26} = 3D_s\Gamma. \tag{B5a,b}$$

(c) Row 3 ($i = 3$) for (2.11*c*)

$$d_{33} = 1, \quad c_{34} = h^2\psi, \quad c_{35} = \tfrac{3}{2}h\psi\Gamma, \quad c_{36} = h\psi^2 + 3D\psi, \tag{B6a–d}$$

$$a_{35} = -3D_s\Gamma, \quad a_{36} = 3sD_s\Gamma. \tag{B7a,b}$$

(d) Row 4 ($i = 4$) for (2.18): note that this equation can be written in a more convenient form to resemble the general form of (B1) as

$$p = -\boldsymbol{\nabla}\cdot\left[\hat{\gamma}(\Gamma, h)\boldsymbol{\nabla}h + \Sigma\frac{\psi^2}{h^3}\boldsymbol{\nabla}h - \Sigma\frac{\psi}{h^2}\boldsymbol{\nabla}\psi\right] + K\frac{\partial F}{\partial h} - K\frac{\psi}{h^2}\frac{\partial F}{\partial \phi}$$
$$+ \beta\left(G - \frac{\psi}{h}\frac{\partial G}{\partial \phi}\right) + \Sigma\left(\frac{2\psi}{h^3}\boldsymbol{\nabla}h\cdot\boldsymbol{\nabla}\psi - \frac{(\boldsymbol{\nabla}\psi)^2}{2h^2} - \frac{3\psi^2}{2h^4}(\boldsymbol{\nabla}h)^2\right), \tag{B8}$$

so that

$$a_{44} = -1, \quad c_{41} = \hat{\gamma} + \Sigma\frac{\psi^2}{h^3}, \quad c_{43} = -\Sigma\frac{\psi}{h^2}, \tag{B9a–c}$$

$$f_4 = -K\frac{\partial F}{\partial h} + K\frac{\psi}{h^2}\frac{\partial F}{\partial \phi} - \beta\left(G - \frac{\psi}{h}\frac{\partial G}{\partial \phi}\right), \tag{B10}$$

$$\beta_{41} = \Sigma\left(\frac{\psi}{h^3}\boldsymbol{\nabla}\psi - \frac{3\psi^2}{2h^4}\boldsymbol{\nabla}h\right), \quad \beta_{43} = \Sigma\left(\frac{\psi}{h^3}\boldsymbol{\nabla}h - \frac{1}{2h^2}\boldsymbol{\nabla}\psi\right). \tag{B11a,b}$$

Here, the term $\nabla h \cdot \nabla \psi$ has been separated into two parts: one as a factor of ∇h (first term in β_{41}) and the other as a factor of $\nabla \psi$ (first term in β_{43}).

(e) Row 5 ($i = 5$) for (2.19)

$$a_{55} = -1, \quad c_{52} = \Sigma_s, \quad f_5 = -\beta_s \frac{\partial G_s}{\partial \Gamma} - K \frac{\partial F}{\partial \Gamma}. \tag{B12a–c}$$

(f) Row 6 ($i = 6$) for (2.20): note that this equation can be written in a more convenient form to resemble the general form of (B1) as

$$\mu = \Sigma \nabla \cdot \left[\frac{\psi}{h^2} \nabla h - \frac{1}{h} \nabla \psi \right] + \frac{K}{h} \frac{\partial F}{\partial \phi} + \beta \frac{\partial G}{\partial \phi} \tag{B13}$$

$$+ \Sigma \left(-\frac{1}{h^2} \nabla h \cdot \nabla \psi + \frac{\psi}{h^3} (\nabla h)^2 \right), \tag{B14}$$

so that

$$a_{66} = -1, \quad c_{61} = -\Sigma \frac{\psi}{h^2}, \quad c_{63} = \frac{\Sigma}{h}, \tag{B15a–c}$$

$$f_6 = -\frac{K}{h} \frac{\partial F}{\partial \phi} - \beta \frac{\partial G}{\partial \phi}, \tag{B16}$$

$$\beta_{61} = \Sigma \left(-\frac{\psi}{2h^2} \nabla \psi + \frac{\psi}{2h^3} \nabla h \right), \quad \beta_{63} = -\Sigma \frac{\psi}{2h^2} \nabla h. \tag{B17a,b}$$

Analogously to the case for $i = 4$, the rectangular term $\nabla h \cdot \nabla \psi$ has been separated into two parts: one as a factor of ∇h (first term in β_{61}) and the other as a factor of $\nabla \psi$ (first term in β_{63}).

This system of equations is solved with periodic boundary conditions in the x-interval $(0, \lambda = 2\pi/k)$.

References

Archer, A.J., Ionescu, C., Pini, D. & Reatto, L. 2008 Theory for the phase behavior of a colloidal fluid with competing interactions. *J. Phys.: Condens. Matter* **20**, 415106.

Archer, A.J., Pini, D., Evans, R. & Reatto, L. 2007 Model colloidal fluid with competing interactions: bulk and interfacial properties. *J. Chem. Phys.* **126**, 014104.

Areshi, M., Tseluiko, D., Thiele, U., Goddard, B.D. & Archer, A.J. 2024 Binding potential and wetting behavior of binary liquid mixtures on surfaces. *Phys. Rev.* E **109**, 024801.

Cahn, J.W. 1965 Phase separation by spinodal decomposition in isotropic systems. *J. Chem. Phys.* **42**, 93–99.

Cahn, J.W. & Hilliard, J.E. 1958 Free energy of a nonuniform system. 1. Interfacial free energy. *J. Chem. Phys.* **28**, 258–267.

Chao, Y., Ramírez-Soto, O., Bahr, C. & Karpitschka, S. 2022 How liquid–liquid phase separation induces active spreading. *Proc. Natl Acad. Sci.* **119**, 2203510119.

Clarke, N. 2005 Toward a model for pattern formation in ultrathin-film binary mixtures. *Macromolecules* **38**, 6775–6778.

Craster, R.V. & Matar, O.K. 2009 Dynamics and stability of thin liquid films. *Rev. Mod. Phys.* **81**, 1131.

Diamant, H. & Andelman, D. 1996 Kinetics of surfactant adsorption at fluid-fluid interfaces. *J. Phys. Chem.* **100**, 13732–13742.

Diez, J.A., González, A.G., Garfinkel, D.A., Rack, P.D., McKeown, J.T. & Kondic, L. 2021 Simultaneous decomposition and dewetting of nanoscale alloys: a comparison of experiment and theory. *Langmuir* **37**, 2575–2585.

Doi, M. 2011 Onsager's variational principle in soft matter. *J. Phys.: Condens. Matter* **23**, 284118.

HUGHES, R.A., MENUMEROV, E. & NERETINA, S. 2017 When lithography meets self-assembly: a review of recent advances in the directed assembly of complex metal nanostructures on planar and textured surfaces. *Nanotechnology* **28**, 282002.

HUTH, R., JACHALSKI, S., KITAVTSEV, G. & PESCHKA, D. 2015 Gradient flow perspective on thin-film bilayer flows. *J. Engng Maths* **94**, 43–61.

JOSEPH, D.D., BAI, R., CHEN, K.P. & RENARDY, Y.Y. 1997 Core-annular flows. *Annu. Rev. Fluid Mech.* **29**, 65–90.

JOSEPH, D.D. & RENARDY, Y.Y. 1992*a* *Fundamentals of Two-Fluid Dynamics. Volume 1: Mathematical Theory and Applications*. Springer.

JOSEPH, D.D. & RENARDY, Y.Y. 1992*b* *Fundamentals of Two-Fluid Dynamics. Volume 2: Lubricated Transport, Drops and Miscible Fluids*. Springer.

KARPITSCHKA, S., LIEBIG, F. & RIEGLER, H. 2017 Marangoni contraction of evaporating sessile droplets of binary mixtures. *Langmuir* **33**, 4682–4687.

KHENNER, M. 2018 Modeling solid-state dewetting of a single-crystal binary alloy thin films. *J. Appl. Phys.* **123**, 034302.

KHENNER, M. & HENNER, V. 2020 Modeling evolution of composition patterns in a binary surface alloy. *Model. Simul. Mater. Sci. Engng* **29**, 015002.

KONDIC, L., GONZALEZ, A.G., DIEZ, J.A., FOWLKES, J.D. & RACK, P. 2020 Liquid-state dewetting of pulsed-laser-heated nanoscale metal films and other geometries. *Annu. Rev. Fluid Mech.* **52**, 235–262.

KÖPF, M.H., GUREVICH, S.V. & FRIEDRICH, R. 2009 Thin film dynamics with surfactant phase transition. *Europhys. Lett.* **86**, 66003.

KÖPF, M.H., GUREVICH, S.V., FRIEDRICH, R. & CHI, L. 2010 Pattern formation in monolayer transfer systems with substrate-medicated condensation. *Langmuir* **26**, 10444–10447.

MAKAROV, S.V., MILICHKO, V.A., MUKHIN, I.S., SHISHKIN, I.I., ZUEV, D.A., MOZHAROV, A.M., KRASNOK, A.E. & BELOV, P.A. 2016 Controllable femtosecond laser-induced dewetting for plasmonic applications. *Laser Photonics Rev.* **10**, 91–93.

MAO, S., KULDINOW, D., HAATAJA, M.P. & KOSMRLJ, A. 2019 Phase behavior and morphology of multicomponent liquid mixtures. *Soft Matt.* **15**, 1297–1311.

MITLIN, V.S. 1993 Dewetting of solid surface: analogy with spinodal decomposition. *J. Colloid Interface Sci.* **156**, 491–497.

MOROZOV, M., ORON, A. & NEPOMNYASHCHY, A.A. 2015 Long-wave Marangoni convection in a layer of surfactant solution: bifurcation analysis. *Phys. Fluids* **27**, 082107.

NÁRAIGH, L.O. & THIFFEAULT, J-L. 2010 Nonlinear dynamics of phase separation in thin films. *Nonlinearity* **23**, 1559–1583.

ORON, A., DAVIS, S.H. & BANKOFF, S.G. 1997 Long-scale evolution of thin liquid films. *Rev. Mod. Phys.* **69**, 931–980.

PARLETT, I.B.N. 1998 *The Symmetric Eigenvalue Problem*. SIAM.

PETERS, G. & WILKINSON, J.H. 1970 $Ax = \lambda Bx$ and the generalized eigenproblem. *SIAM J. Numer. Anal.* **7**, 479–492.

PODOLNY, A., ORON, A. & NEPOMNYASHCHY, A.A. 2005 Long-wave Marangoni instability in a binary-liquid layer with deformable interface in the presence of Soret effect: linear theory. *Phys. Fluids* **17**, 104104.

POTOTSKY, A., BESTEHORN, M., MERKT, D. & THIELE, U. 2004 Alternative pathways of dewetting for a thin liquid two-layer film. *Phys. Rev.* E **70**, 025201.

POTOTSKY, A., BESTEHORN, M., MERKT, D. & THIELE, U. 2005 Morphology changes in the evolution of liquid two-layer films. *J. Chem. Phys.* **122**, 224711.

SARIKA, C.K., TOMAR, G. & BASU, J.K. 2016 Pattern formation in thin films of polymer solutions: theory and simulations. *J. Chem. Phys.* **144**, 024902.

SARIKA, C.K., TOMAR, G., BASU, J.K. & THIELE, U. 2015 Bimodality and re-entrant behaviour in the hierarchical self-assembly of polymeric nanoparticles. *Soft Matt.* **11**, 8975–8980.

SHARMA, A. & JAMEEL, A.T. 1993 Nonlinear stability, rupture and morphological phase separation of thin fluid films on polar and polar substrates. *J. Colloid Interface Sci.* **161**, 190–208.

SHARMA, A., KISHORE, C.S., SALANIWAL, S. & RUCKENSTEIN, E. 1995 Nonlinear stability and rupture of ultrathin free films. *Phys. Fluids* **7**, 1832–1840.

SHKLYAEV, S., NEPOMNYASHCHY, A.A. & ORON, A. 2009 Marangoni convection in a binary liquid layer with soret effect at small lewis number: linear stability analysis. *Phys. Fluids* **21**, 054101.

SHKLYAEV, S., NEPOMNYASHCHY, A.A. & ORON, A. 2013 Oscillatory longwave marangoni convection in a binary liquid: rhombic patterns. *SIAM J. Appl. Maths* **73**, 2203–2223.

SHKLYAEV, S., NEPOMNYASHCHY, A.A. & ORON, A. 2014 Oscillatory longwave Marangoni convection in a binary liquid. Part 2: square patterns. *SIAM J. Appl. Maths* **74**, 1005–1024.

STRANG, G. 1988 *Linear Algebra and Its Applications*, 3rd edn. Harcourt Brace Jovanovich College Publishers.

THIELE, U. 2011 Note on thin film equations for solutions and suspensions. *Eur. Phys. J. Spec. Top.* **197**, 213–220.

THIELE, U. 2018 Recent advances in and future challenges for mesoscopic hydrodynamic modelling of complex wetting. *Colloids Surf.* A **553**, 487–495.

THIELE, U., ARCHER, A.J. & PISMEN, L.M. 2016 Gradient dynamics models for liquid films with soluble surfactant. *Phys. Rev. Fluids* **1**, 083903.

THIELE, U., ARCHER, A.J. & PLAPP, M. 2012 Thermodynamically consistent description of the hydrodynamics of free surfaces covered by insoluble surfactants of high concentration. *Phys. Fluids* **24**, 102107.

THIELE, U., MADRUGA, S. & FRASTIA, L. 2007 Decomposition driven interface evolution for layers of binary mixtures. I. Model derivation and stratified base states. *Phys. Fluids* **19**, 122106.

THIELE, U., TODOROVA, D.V. & LOPEZ, H. 2013 Gradient dynamics description for films of mixtures and suspensions: dewetting triggered by coupled film height and concentration fluctuations. *Phys. Rev. Lett.* **111**, 117801.

THIELE, U., VELARDE, M.G. & NEUFFER, K. 2001 Dewetting: film rupture by nucleation in the spinodal regime. *Phys. Rev. Lett.* **87**, 016104.

THOMPSON, C.V. 2012 Solid-state dewetting of thin films. *Annu. Rev. Mater. Res.* **42**, 399–434.

TODOROVA, D.V. 2013 Modelling of dynamical effects related to the wettability and capillarity of simple and complex liquids. PhD thesis, Loughborough University.

XU, X., THIELE, U. & QIAN, T. 2015 A variational approach to thin film hydrodynamics of binary mixtures. *J. Phys.: Condens. Matter* **27**, 085005.